2010

Computer-Based Skeletal Age Assessment Using Hand/Wrist Radiographs in Children 8-18 Years Old

Zhihong Ni
Wright State University

COMPUTER-BASED SKELETAL AGE ASSESSMENT

USING HAND/WRIST RADIOGRAPHS

IN CHILDREN 8-18 YEARS OLD

A thesis submitted in partial fulfillment
of the requirements for the degree of
Master of Science in Engineering

By

ZHIHONG NI
B.E., Tianjin Medical University, 2007

2010
Wright State University

WRIGHT STATE UNIVERSITY

SCHOOL OF GRADUATE STUDIES

August 17, 2010

I HEREBY RECOMMEND THAT THE THESIS PREPARED UNDER MY SUPERVISION BY Zhihong Ni ENTITLED Computer-based Skeletal Age Assessment Using Hand/Wrist Radiographs in Children 8-18 Years Old BE ACCEPTED IN PARTIAL FULFILLMENT OF THE REQUIREMENTS FOR THE DEGREE OF Master of Science in Engineering.

____

Thomas N. Hangartner, Ph.D.
Thesis Advisor

____

Thomas N. Hangartner, Ph.D.
Interim Department Chair

Committee on Final Examination

____

Thomas N. Hangartner, Ph.D.

____

Dana L. Duren, Ph.D.

____

Julie A. Skipper, Ph.D.

____

Andrew T. Hsu, Ph.D.
Dean, School of Graduate Studies

ABSTRACT

Ni, Zhihong. M.S.E., Department of Biomedical, Industrial & Human Factors Engineering, Wright State University, 2010. Computer-based Skeletal Age Assessment Using Hand/Wrist Radiographs in Children 8-18 Years Old.

Children's skeletons mature at different rates, and they can be affected by a variety of factors including disease, hormone imbalance or genetics. The assessment of skeletal maturity is a frequently performed procedure that allows the detection of hormonal, growth or genetic disorders. Several methods have been developed to estimate skeletal maturity. Most methods evaluate hand/wrist radiographs using indicators such as the ratios of various bone widths, the onset of the ossification of epiphysis and epiphyseal-diaphyseal fusion. Among those methods, the FELS method differs from others in the application of different grades to each indicator and the provision of a confidence limit of the determined skeletal maturity.

However, skeletal age assessment based on the FELS method, as with any method, is associated with observer variability. There is also increased pressure on pediatric radiologists to read more and larger sets of radiographs. These problems could be solved by an automated computerized method, which has the potential to reduce the time required to examine the image and to increase the reliability of the analysis. The aim of this project is the development of an automated computer-based analysis method to estimate skeletal age from hand/wrist radiographic images. Such images were obtained through not only traditional x-ray procedures but also from a dual x-ray absorptiometry scanner. The analysis was performed in several stages: the

preprocessing step, the ROI extraction step and the indicator analysis step. The results obtained from the analysis were then integrated and used to calculate the skeletal age and its associated standard error.

In this study, 174 left hand/wrist radiographs of children between the ages of 8 and 18 years were selected from the FELS Longitudinal Study; 100 of them were used for training and the remainder for testing. DXA images of the participants in the testing set were used to evaluate the possibility of assessing skeletal age based on DXA. The automated analysis was successful in approximately 90% of the training set, 85% of the testing set and 100% of the DXA image set. Manual intervention of the ROIs localization allowed the remaining images to be analyzed.

The grades of all the indicators together with the skeletal age of each participant generated from our analysis method were compared with the reference values provided by two well trained specialists at the Lifespan Health Research Center. Most of the indicators (85%) do not show statistical differences between the observation values obtained from our program and the reference values. By comparing the skeletal age estimated by our program and by the specialists, it was found that the analysis of the traditional x-ray images was fairly good; only 13.3% of the training set and 20.6% of the testing set show differences that are larger than one year. However, the results of the DXA images were worse; about 40.5% of this data set show a difference larger than one year. In addition, the indicators that could not be graded by our program do have some effect on the skeletal age assessment of the children from 8 to 18 years old.

TABLE OF CONTENTS

LIST OF FIGURES

LIST OF TABLES

ACKNOWLEDGEMENTS

First of all, I would like to express my intense gratitude to my advisor Dr. Thomas N. Hangartner, who introduced me to the field of biomedical image processing. His knowledge, support, guidance and encouragement were really critical to me. Without him and his help this thesis would have been impossible to complete.

My special thanks also go to Dr. Dana L. Duren, who has been spending a lot of time helping me understand the basic concept of skeletal-age assessment and interpreting my results.

I am grateful to Dr. Julie A. Skipper for her valuable suggestions and help at the beginning of this project and also for her precious time in reviewing this thesis.

I am thankful to Ms. Sharon Lawrence and Mr. Joseph Wagner, Research Assistants, Department of Community Health, who have put in a lot of effort in training me to successfully assess the skeletal age and helping me get the results from my dataset.

I also would like to thank the faculty and staff of the Department of Computer Science and Engineering at Wright State University for giving me lots of guidance and assistance.

Last but not least, I would like to thank my husband Wei Ye. His sacrifice, support, encouragement and love made it possible for me to complete this project.

Dedicated to

My Parents and My Husband

Chapter 1

Introduction

Children's skeletons mature at different rates. Skeletal maturity can be affected by a variety of factors including disease, hormone imbalance or genetics. The assessment of skeletal maturity plays an important role in pediatric radiology. It is a frequently performed procedure that allows the detection of hormonal, growth or genetic disorders. Based on a radiological examination of skeletal development of the hand/wrist, skeletal maturity (a.k.a., "skeletal age" or "bone age") is assessed and then compared with the child's chronological age. A large difference between these two values indicates abnormalities in skeletal development. A delayed or accelerated maturation can be reflected in the calculated difference between chronological and skeletal ages. Because of the importance of skeletal maturity, several methods have been developed for estimating skeletal age. Most of the methods evaluate the hand/wrist radiographs using indicators such as the ratios of the width of epiphysis versus metaphysis in various bones, the onset of bone ossification and the degree of epiphyseal-diaphyseal fusion. In the most commonly used methods, such as the Tanner and Whitehouse (TW2) method[1] and the Greulich and Pyle (G&P) method,[2] the left hand/wrist radiological examination is used due to its simplicity, minimal radiation exposure, and the availability of multiple ossification centers for evaluation of maturity.[3]

In the 1980's, the FELS method[3] was developed by Roche, Chumlea and Thissen as an alternative method for assessing skeletal age. This method differs from others in the application of different grades to each indicator and the provision of a confidence limit of the determined skeletal maturity. The FELS method is based on serial left hand/wrist radiographs of Caucasian children in the Fels Longitudinal Study.[4] Comparison among the skeletal age assessments for children in the Fels Longitudinal Study by the FELS, G&P, and TW2 methods indicate that the FELS method is the most appropriate method for the present population of United States children.[5]

However, all the commonly used methods of the skeletal age assessment are associated with considerable observer variability. There is also increased pressure on pediatric radiologists to read more and larger sets of radiographs. These problems could be solved by an automated computerized method, which has the potential to reduce the time required to examine the image and to increase the reliability of the analysis. Because of its many advantages over other methods, the FELS method provides the ideal assessment method upon which to base this automation. It is also potentially possible to assess skeletal age based on an image created by the newer models of dual-x-ray absorptiometry (DXA) scanners, which deliver less radiation exposure than other tests, such as CT scans or radiographic absorptiometry.

The goal of this project is the development of an automated computer-based analysis method to estimate skeletal age of children 8-18 years old from left hand/wrist radiographic images. Such images could be obtained through not only the traditional x-ray procedures but also using DXA scanners.

The analysis starts with a series of preprocessing steps, which is used to correct the image orientation and remove unwanted background. The next procedure of the analysis is localization of the regions of interest (ROI), which can extract all the bones of interest in a digitized hand/wrist radiograph. Then, the indicators of each bone are analyzed by a sequence of image processing algorithms. The last part of the computer-based analysis is the aggregation of all indicator grades, which can estimate the skeletal age of a child and provide a standard error value.

Chapter 2

Background

2.1 Definition of Skeletal Age

There are two ages of a child: the chronological age and the skeletal age. The chronological age is the actual age in years, determined from the child's birth date. The skeletal age describes the degree of maturation of a child's bones.[6] Skeletal age is the age at which an average child reaches a particular stage of bone maturation. Since individual growth rates vary, the skeleton of children of the same chronological age may show marked differences in maturity. However, changes in human skeletal development are basically similar, as the development process of each bone has continuity and runs through the same stages.[4] At each stage, bones have specific characteristics. Therefore, comparing with chronological age, skeletal age assessment is a more accurate way to reflect the level of individual growth development and the degree of maturation. The skeletal age can not only be used to determine the biological age but also help to understand the potential for growth and development of children.[7]

2.2 Significance of Skeletal Age Assessment

The development of the skeleton is of great importance to the health and maturation of a growing child. Bone development is influenced by a number of factors, including nutrition, hormonal secretions and genetics. Abnormality of skeletal development is usually one aspect of the manifestation of some pediatric endocrine diseases. For this reason, skeletal age assessment is critical for the analysis of growth disorder and plays an important role in pediatrics. This procedure is frequently performed in the management and diagnosis of endocrine disorders as well as the monitoring of growth hormone therapy.[6] Bone age determination is also commonly used to predict individual's final height.[7]

2.3 Fundamental Principles of Skeletal Age Assessment

The methods of assessing skeletal age from radiographs are based on the recognition of maturity indicators. Maturity indicators are radiographic features of bone shape that reflect the three-dimensional shapes of the external surface of bones.[4] These surfaces change shape during maturation as bone replaces the cartilaginous anlage. In the TW2 and G&P methods, skeletal age is assessed by analyzing ossification centers in the carpal bones and epiphyses in the tubular bones, which include distal, middle, and proximal phalanges, metacarpals, as well as ulna and radius (Figure 2.1). Among these, the stage of epiphyseal development is the most relevant bony structure considered in an assessment of skeletal maturity.[4] In the examination, the patient's left hand/wrist radiograph is compared with established patterns for a given bone age.

Figure 2.1. Hand wrist radiograph

2.4 Commonly Used Methods and the Problems

Currently, the main clinical methods for skeletal bone-age evaluation are the TW2 method and the G&P method.[1,2] The TW2 method is usually considered the more accurate and reliable method of the two, because it uses a detailed analysis of each individual bone, which is described in terms of scores. This method is acknowledged as more objective than the G&P method; however, it is more time consuming, and thus the rate of its application does not exceed 20%.[8] The G&P method compares the left hand/wrist radiograph with the patterns in a picture atlas. The pattern that superficially resembles the clinical image most closely is selected. Since each pattern is assigned to a certain year of age, the selection determines the skeletal age. This method is rather subjective and gives more random variation, but it is used more frequently (76%)[9] due to its simplicity in comparison with TW2. Furthermore, in order to produce reliable results, a well trained observer is required, and the maturity stages of different bones have to be carefully evaluated.

2.5 The FELS Method

FELS Method was developed by Roche, Chumlea and Thissen[3] in order to provide an objective assessment of skeletal age together with a confidence limit, which can be reflected by a standard error. The measurement of skeletal age using FELS method from a radiograph depends upon the recognition of maturity indicators. These indicators are radiographically visible features of bones that undergo successive changes during maturation. Most of the indicators reflect the replacement of cartilage by bone, but some are due to growth of the bone at subperiosteal surfaces or the resorption of bone.[10] Each of these mechanisms causes changes that can be recognized radiographically from alterations in the outlines of bones or the presence of radiopaque lines or zones.

The data for developing this method were based on 13,823 serial radiographs of the left hand/wrist of 355 boys and 322 girls born between 1928 and 1974, enrolled in the Fels Longitudinal Study.[4] The radiographs that were used to develop the FELS method included about 3 cm of the distal ends of the radius and ulna as well as the hand. These radiographs were distributed evenly by age, except for smaller numbers at the half-years after 14 years and at 20 and 22 years. The radiographs were taken from one month to 22 years of age. The visit schedule for each Fels participant was as follow: from birth to age one year, data were collected every three months; from the age of one year to 18 years, data were collected every six months; from 18 years onward the time interval became two years.[10] All analyses were performed for each sex separately.

When developing the FELS method, the usefulness of all possible hand/wrist indicators was determined first. Next, as with grading method, the indicators of each bone of the hand/wrist were evaluated individually. A total of 22 bones and 98 available indicators were chosen in the method. Then, data derived from all useful maturity indicators were combined into a single estimate of skeletal age with the standard error of that estimate by a weighting system. The standard error is a measure of the confidence limit of a specific age due to the variability of the age relationship of the various indicators.[11] The method they developed to grade different kinds of indicators will be discussed in a later section.

Chapter 3

Materials and Methods

3.1 Database

In this research project, 174 left hand/wrist radiographs of children between the ages of 8 and 18 years were selected from the Fels Longitudinal Study; 100 of them were used as the training set and the remainder for testing. A VIDAR Dosimetry PRO Advantage® film digitizer (VIDAR Systems Corporation, Herndon, VA) was used to digitize the films. This digitizer provides a nominal 16-bit grayscale resolution and 300 dpi (85 μm pixel size) spatial resolution. Furthermore, 74 DXA left hand/wrist images were also involved in this project. These images were taken with a Hologic QDR 4500 Discovery A DXA scanner (Hologic, Inc., Bedford, MA) at the same time when the 74 children of the testing set underwent the traditional hand/wrist radiograph procedure. All procedures were approved by Wright State University's Institutional Review Board, and informed consent was obtained from the subjects and/or parents prior to any procedure.

3.2 Image Preprocessing

A number of algorithms for hand/wrist analysis exist in the literature related to skeletal age assessment.[12-14] They all deal with the problem of segmenting certain regions within the radiograph; however, a rather low accuracy of the region detection may result in these algorithms if images were not adequately preprocessed. To avoid this inaccuracy, nonuniformity of the image background should be suppressed, since a uniform background can improve threshold-based region definitions. Depending on the type of region to be identified, the imaged soft tissue may also be considered the background relative to the bones and need to be suppressed. Another preprocessing function not being considered by the previous algorithms is the hand orientation. Authors at times defined a “standard” hand position (for their approach) that varied from the medically accepted standard position.[15]

In order to prepare an image for computerized analysis, a preprocessing function is first implemented in the current project to standardize images. This function includes several distinct steps. First, the images ware classified based on histogram analysis, and brightness and contrast are enhanced. Second, the background is eliminated to increase the hand-to-background ratio and standardize the image values. Third, the image orientation is corrected to ensure a standard hand position within the image. Last, the bones of interest are extracted and prepared for the following indicator analysis steps.

3.2.1 Image Classification

Since the Fels participants were involved in a longitudinal study, there is variation among the quality of images. Some of them were overexposed and of poor contrast. Consequently, some images require a particular grayscale-adjustment step. In order to let the program automatically recognize the images with poor contrast and implement the adjustment function, the image histogram is used to assess the quality of that image. An image histogram is a chart that shows the distribution of intensities in a grayscale image. Since the images used in this study are digitized with a depth of 16-bit, the range of the histogram is from 0 to 65535.

By knowing the histogram of an image, a cumulative distribution function (CDF)[16] can be calculated to help recognize an overexposed image. In our study, 95% of the CDF is used as a cut-off gray value. If this cut-off value is lower than 30,000, the image is classified as overexposed with poor contrast(Figure 3.1).

a)

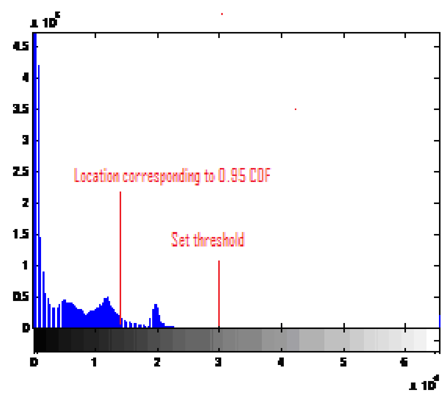

b)

Figure 3.1. Over exposed image. a) An overexposed image having low contrast; b) the histogram of the image showing that the grayscale value corresponding to 0.95 CDF lies below the set threshold of 30,000.

For the images that were overexposed, a logarithmic transformation was applied in order to spread the gray values of the image across a wider range (Figure 3.2). This adjustment can help to generate an image with good contrast, for which it will be easier to find an appropriate segmentation threshold later.

a) b)

Figure 3.2. Application of logarithmic transformation. a) Low contrast image before and b) after application of logarithmic transformation.

3.2.2 Elimination of Background

There are various definitions of background. First, in the preprocessing steps, background is referred to as an area outside the patient body and within the radiation field. This kind of background varies from different films due to the exposure level of the scanning, and it is always nonuniform. In addition, landmarks or labels with patient demographic data (name, birthday, ID number, etc.) may also be found in this area (Figure 3.3a). Second, in the indicator analysis steps, a different background definition is considered. It is referred to the soft tissue surround the bone of interest, which can highly affect the accuracy of indicator grading and therefore also need to be suppressed. The elimination of the second kind of background will be mentioned in the later section.

The basic goal of our first analysis step is to determine the location of the hand in the image. This goal can be achieved in two stages. First, the nonuniform background outside the patient body is estimated and subtracted from the hand image. Second, the image is transformed into a binary mask, and the high-intensity artifacts (labels, markers and wedges) are separated and removed from the image.

Background Estimation and Suppression

Successful extraction of the hand requires an increase of the hand-to-background gray level ratio. Although we have already adjusted the contrast of some poor-quality images in the "Image Classification" step, there is still considerable background nonuniformity caused by the heel effect of the x-ray tube, which makes the following image analysis steps problematic. The heel effect originates from the angled anode, producing a reduced x-ray-beam intensity on the anode side compared to the cathode side and resulting in a gray-level gradient across the film. In most hand/wrist images, the nonuniform background makes it difficult or even impossible to separate the hand area using a single gray-level threshold. Thus, background estimation and suppression, resulting in background equalization, are employed.

First, the four corners of the image are extracted after dividing the image into nine equal regions, and an averaging filter with 5x5 pixel size is implemented in these areas in order to smooth them. Within each corner region, the low gray values (less than 20,000) correspond to the background, whereas the high gray values reflect the soft and bony tissue in that region. Second, one value is selected for each region, corresponding to the bin that represents the peak of the histogram below 20,000. Third, in each corner region, we pick one pixel from the pixels with the selected values, and the chosen pixel will have the shortest distance from the corner of the original whole image. Thus, we can get a total of four pixels from the four corner regions, which are: $A_1(x_{11},y_{11},z_{11})$, $A_2(x_{12},y_{12},z_{12})$, $B(x_2,y_2,z_2)$ and $C(x_3,y_3,z_3)$. The three parameters of each pixel reflect their locations in the original image (the values of *x* and *y*) and their gray values (the value of *z*).

Then, the first two pixels A_1 and A_2, which came from the upper-left and upper-right corner regions of the image, are combined to generate a new pixel $A(x_1,y_1,z_1)$ between them. The equation used to calculate the location and gray value of the new pixel A is:

$$\begin{cases} x_1 = \frac{1}{2}(x_{11} + x_{12}) \\ y_1 = \frac{1}{2}(y_{11} + y_{12}) \\ z_1 = \frac{1}{2}(z_{11} + z_{12}) \end{cases} \tag{3.1}$$

Using the locations and gray values of pixels A, B and C, we can calculate the gray value Z of all pixels in the background located at (*X, Y*) by the following equation:

$$\begin{cases} X = x_1 + u(x_2 - x_1) + v(x_3 - x_1) \\ Y = y_1 + u(y_2 - y_1) + v(y_3 - y_1) \\ Z = z_1 + u(z_2 - z_1) + v(z_3 - z_1) \end{cases} \tag{3.2}$$

The parameters *u* and *v* are calculated from the equations for *X* and *Y* and are applied to the equation for Z.

Then the estimated background (Figure 3.3b) is subtracted from the original image (Figure 3.3a), and a new image with more uniform background is generated (Figure 3.3c).

This background estimation method assumes linear gradients in the horizontal and vertical directions of the image. It can not estimate the exact gray level of every pixel of background outside the hand, which might be affected by many other factors, but it was shown to be useful enough to suppress the background.

a) b) c)

Figure 3.3. Background estimation and suppression. a) Original image with nonuniform background; b) estimated background using equation 2; c) new image with uniform background after background suppression.

Hand Object Extraction

The extraction of the hand is based on thresholding. A threshold value can be set by using a modified version of Matlab's *graythresh* function, which applies Otsu's method to select an optimal threshold to minimize the interclass variance of the black and white pixels.[17] The thresholding procedure turns pixel values lower than the threshold value to zero, which means black, and changes pixel values larger than the threshold to one, which means white (Figure 3.4b). Considering all the connected white pixels of the image as one object, there are several objects in the image, and the hand should be the largest one. In order to remove the smaller noisy elements of the background, the largest object is identified based on Matlab's *bwlabel* function, which assigns different labels to connected components in 2-D binary image. The pixels of all other smaller objects are turned to zero. After this step, a new mask is created (Figure 3.4c). A logical AND operation combining the original image and the mask generates a standard hand wrist image without unwanted background outside the patient body (Figure 3.4d).

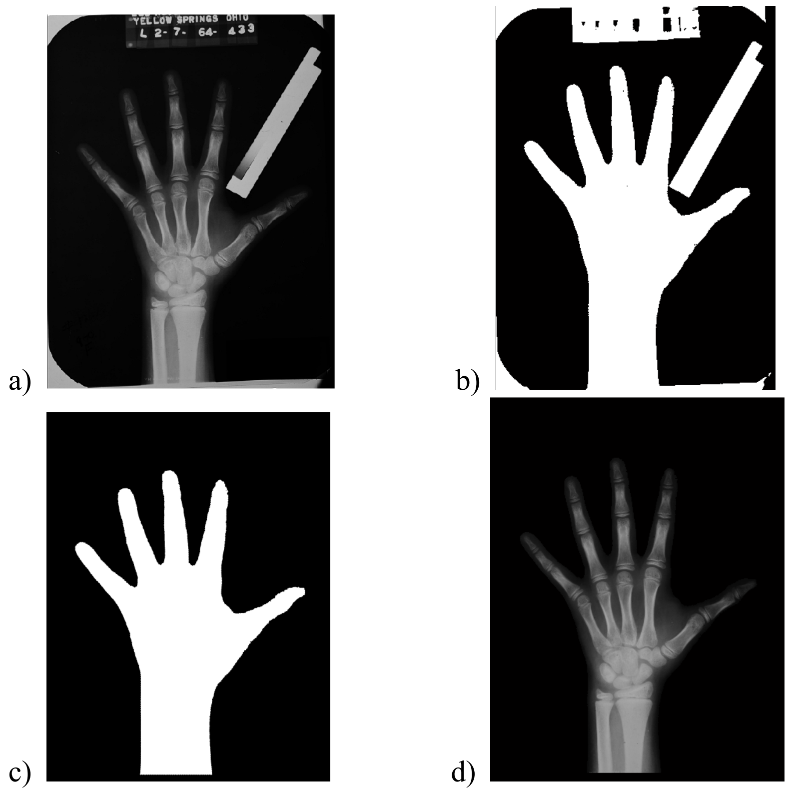

Figure 3.4. Hand mask and background removal. a) Original image with unwanted background; b) binary image created by thresholding; c) mask of the hand/wrist; d) a standard hand/wrist image without unwanted background outside the patient body.

3.2.3 Orientation Correction

The position viewed by radiologists (Figure 2.1) is considered a standard orientation. However, a film cassette might be placed in various positions to best accommodate the examination condition. About 20% of the films in the current data set were generated from procedures that were not performed with the standard image orientation, and these films can be further divided into two types (I and II) depending on whether an angle exists between hand and forearm (Figure 3.5a and 3.5b). It is necessary to orient these images before further analysis is performed.

First, for both of these two types of images, the midline of the forearm can be set as a reference line, which is obtained from the mask image (Figure 3.4c). A new image with the standard orientation of the forearm is then created by rotating the original image to make the reference line vertical. The result of the orientation correction is shown in Figures 3.5c and 3.5d.

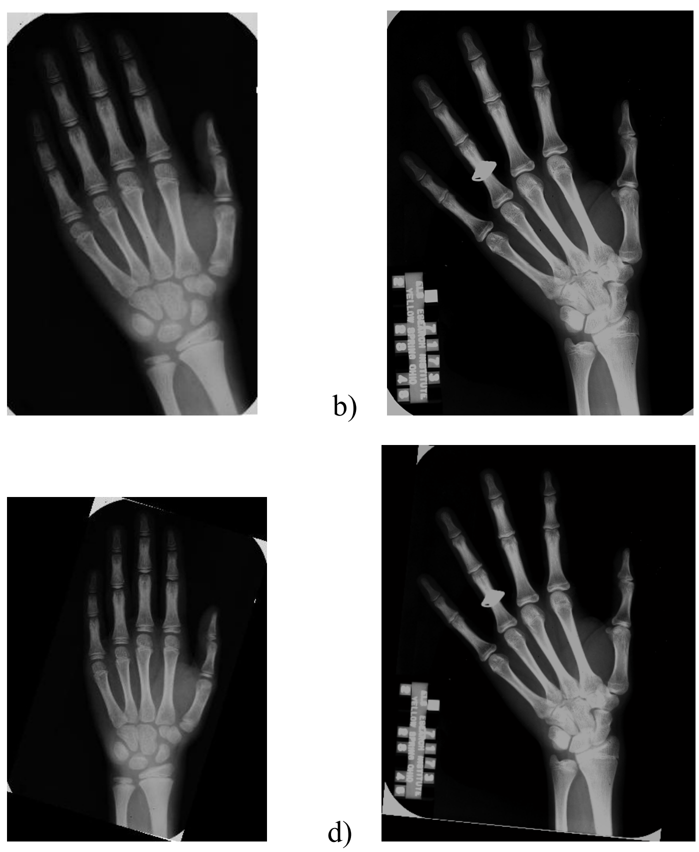

a) b)

c) d)

Figure 3.5. Orientation correction (step I). a) Original image with unconventional orientation Type I; b) original image with unconventional orientation Type II; c) new image after orientation correction of a); d) new image after orientation correction of b).

Second, for the Type II images, one more rotation must be performed in order to generate the standard orientation of the hand. In this step, the tip of the third phalanx, together with the mid point of the line on the hand-forearm junction can be used to generate a reference line. In order to obtain the line on the hand-forearm junction, we use the vertically flipped mask image (Figure 3.6a) to get a profile showing the number of white points on each row of the image (Figure 3.6b). After removing the first several zero points of the profile (Figure 3.6b), the differences between adjacent elements of this profile are calculated (Figure 3.6c). The row of the hand-forearm junction shows a larger difference value. The center of this line within the mask and the tip of the third phalanx define the reference line, which is used to align the hand part vertically (Figure 3.6d).

a) 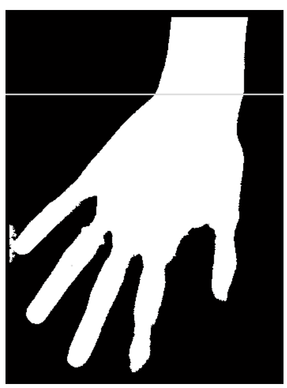

b) 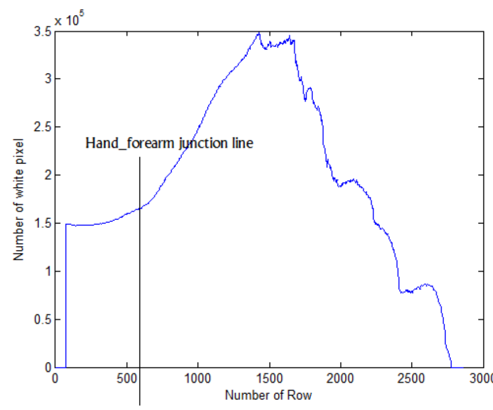

c) 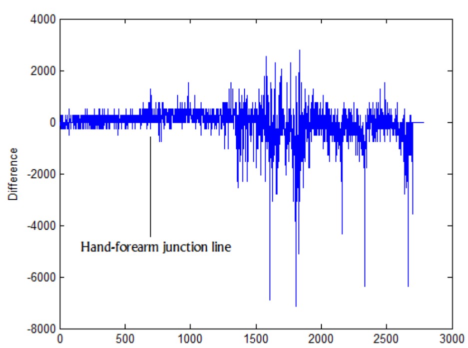

d) 

Figure 3.6. Orientation correction (step II). a) Mask of Figure 3.5b after vertical flip; b) profile showing the number of white points in each row of a); c) differences between adjacent elements of b); d) hand part after orientation correction of Figure 3.5b.

3.3 Localization of Bones of Interest

Following hand segmentation, the next task is to identify all the bones which need to be graded in the FELS method. To achieve this, we divide the original hand/wrist image into three regions of interest (ROI): forearm ROI, phalanges ROI and metacarpals ROI, and then we segment all the bones of interest within each region.

3.3.1 Forearm ROI Extraction

In the orientation correction section, we talked about how to locate the hand-forearm junction line of the Type II images. For the Type I images and other images that were generated using the standard image orientation (Figure 3.7a), we can use the same method to locate the junction line and to extract the forearm region (Figure 3.7b). In this region there are two bones to be graded in the FELS method: radius and ulna. To segment these two bones from the forearm image, we use the profile of a row, which is 100 rows above the bottom line of the image (the white line in Figure 3.7b). The profile of that row is shown in Figure 3.7c. On this profile, we can easily identify the two peaks, which reflect the ulna region and radius region. The line in the middle of these two regions is used to segment the radius and ulna (Figure 3.7d and 3.7e).

After running the hand-forearm junction line detection and orientation correction procedures, we obtain an image of the hand with standard orientation (Figure 3.8a). Using the mask of this hand image, we can identify the phalanges region by detecting two lines as shown on Figure 3.8a. The upper line is at the tip of the third phalanx. Since we have already rotated the hand to a standard orientation, the tip of the third phalanx can be detected as the highest positioned white point in the image. The second line can be detected by counting the zero crossings of each row of the mask.[16]

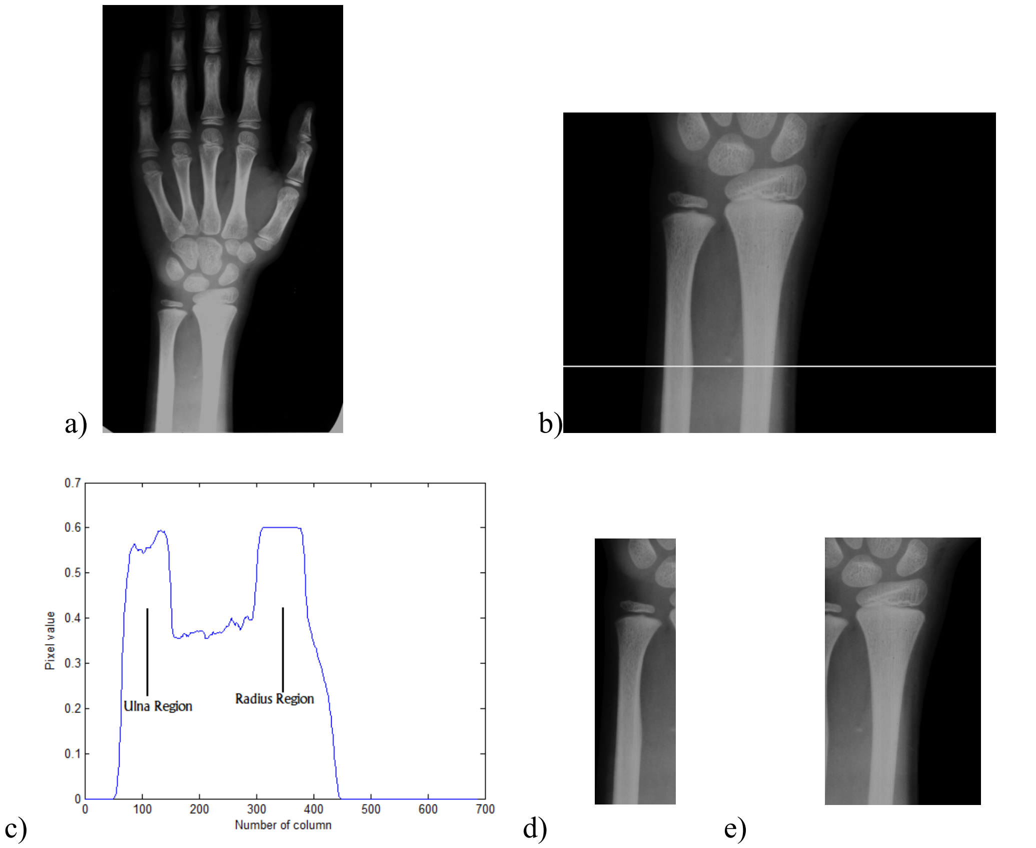

Figure 3.7. Segmentation of radius and ulna. a) Original image; b) forearm ROI extraction; c) profile of the white line on b); d) ulna segmentation; e) radius segmentation.

A zero crossing for our purpose is a transition from an ON pixel (gray value = 1) to an OFF pixel (gray value = 0) or vice versa. By progressively analyzing rows from the finger region to the palm region, the number of zero crossings decreases. The lower line in Figure 3.8b shows the row where the number of zero crossings first falls below four. By using this line together with the top line (the tip of phalanx III), we can segment the phalangeal ROI (Figure 3.8c). We also add a fixed number of rows as a buffer to ensure that the proximal ends of phalanges I and V are properly included in the segmented ROI.

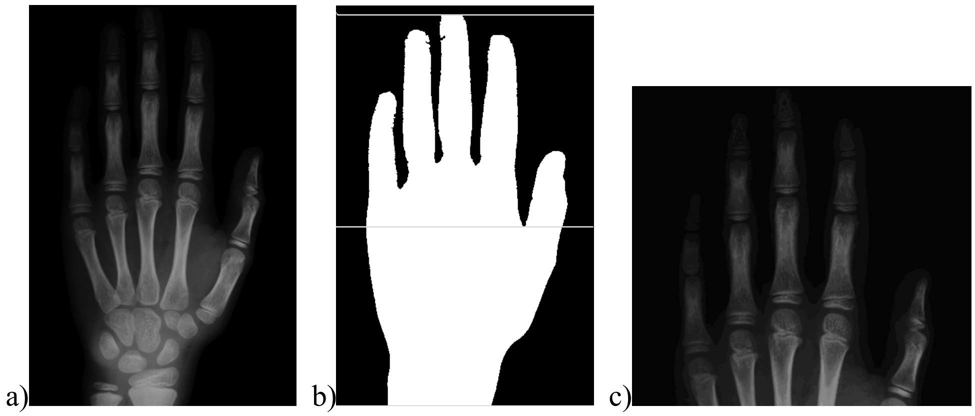

Figure 3.8. Segmentation of phalanges ROI. a) The hand part of Figure 8a; b) mask of a) with two lines used to segment the phalanges ROI; c) phalanges ROI.

Using the binary image of the phalanges ROI, scanning rows from the top of the image, we can get the tips of the first (when the number of zero crossings exceeds 8), third and fifth phalanges (when the number of zero crossings exceeds 6). Since the phalangeal width always falls into a range of less than 300 columns, we can use the phalangeal tips together with the bottom line of the phalanges ROI (Figure 3.8c) to create a bounding box with a constant width in order to segment the phalanges we want (the first, third and fifth phalange) from the rest of the image (Figure 3.9a, b and c).

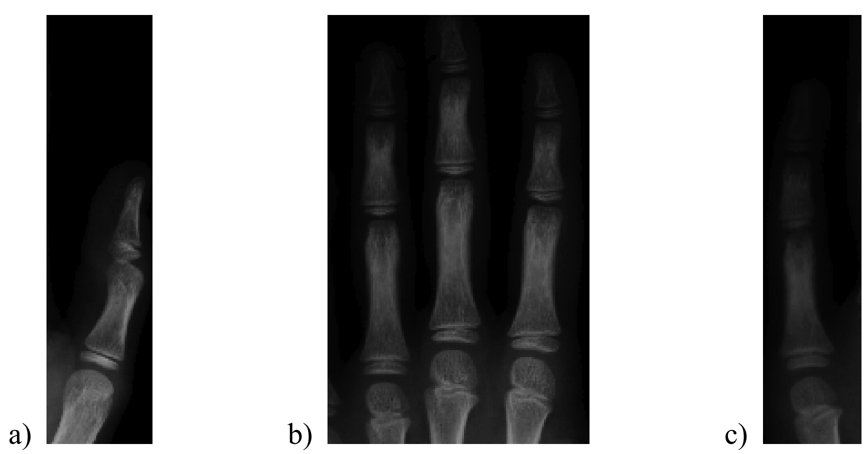

Figure 3.9. Phalanx I, III and V extraction. a) The first phalanx ROI; b) the third phalanx ROI; c) the fifth phalanx ROI.

It should be noted that, for the third phalanx ROI, the phalanges located beside the third one are also included in the extracted region. This fact can help to successfully segment the entire third phalanx, taking into account that the third phalanx is usually diagonal. Additional phalanx segmentation in that region is handled through subsequent processing steps.

Proximal, Middle and Distal Parts of Phalanx III Extraction

In order to segment the three parts of Phalanx III, we first use the same method as described in the “Image Classification” section to adjust the gray levels of the third phalanx ROI (Figure 3.10a). This step aims to improve image contrast and aids in finding an appropriate segmentation threshold later. To segment the phalanx of interest, two binary masks are created. The first one is obtained by thresholding the adjusted third phalanx ROI (Figure 3.10a) based on Otsu’s method (Figure 3.10b). The second one is obtained by first creating the boundary of the features within the ROI using Matlab’s edge detection function and then filling the holes inside the boundary (Figure 3.10c). An “OR” logic operation is applied to the upper three quarters of these two binary images in order to obtain the whole phalange of interest; then, an “AND” logic operation is applied to the lower one quarter of the two binary images in order to separate the metacarpal region and help to segment the third phalanx (Figure 3.10d).

Next, all the objects inside the combined binary image (Figure 3.10d) are labeled by considering all the connected white pixels in the image as one object. The object in the middle of the image should be the phalanx of interest and is extracted as the mask of Phalanx III (Figure 3.10e).

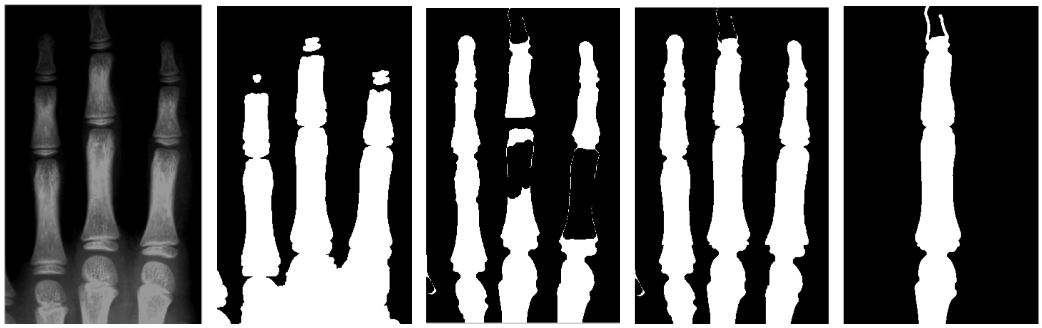

a) b) c) d) e)

Figure 3.10. Three parts of Phalanx III extraction (step I). a) Adjusted Phalanx III ROI; b) binary mask of a) generated by thresholding based on Otsu's method; c) binary mask of a) generated by filling the holes of edges obtained by edge detection function; d) combination of b) and c) using "AND" and "OR" logic operation; e) mask of Phalanx III.

The following step uses the background-removal function to remove the soft tissue in the Phalanx III ROI as much as possible. The background removal function includes the following steps: First, apply an averaging filter of k x k pixels (k = 20 here) to the adjusted Phalanx III ROI (Figure 3.10a) in order to estimate the value of the background pixels (Figure 3.11a); second, subtract the estimated background (Figure 3.11a) from the adjusted Phalanx III ROI (Figure 3.10a) to create an image with a uniform background (Figure 3.11b); third, adjust the brightness in the processed image (Figure 3.11c); fourth, use an "AND" logical operation to combine Figure 3.11c and Figure 3.10e together in order to generate an image includes the third phalanx bone tissue only (Figure 3.11d).

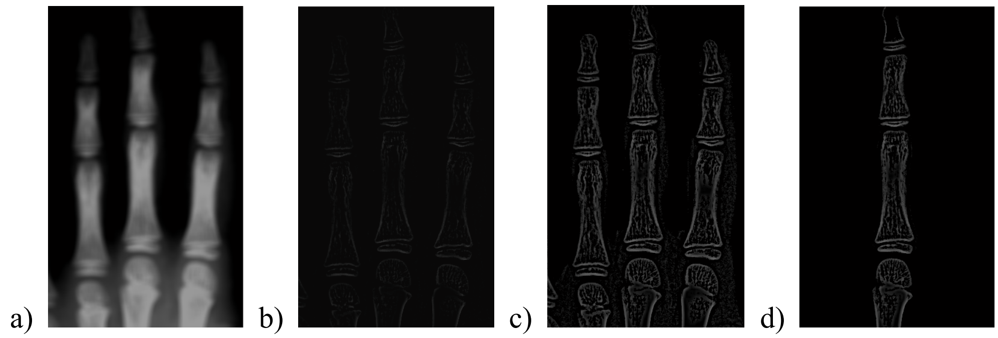

Figure 3.11. Three parts of Phalanx III extraction (step II). a) Estimated background of Figure 11a; b) new image with an uniform background after subtracting Figure 12a from Figure 11a; c) adjust the contrast in Figure b); d) combination of c) and Figure 11e using “AND” logical operation.

Using the processed image (Figure 3.11d) and applying several morphological operations such as filling holes, opening and closing, we can obtain a binary image of Phalanx III without soft tissue (Figure 3.12a). In this image, the biggest object is the proximal part of Phalanx III, and it can be segmented by using the “label” function as mentioned above (Figure 3.12b). Furthermore, by knowing the label value of the proximal part of Phalanx III, we can also get the label value of the middle and distal parts of Phalanx III (the two objects right above the proximal part) and segment them separately from the Phalanx III ROI (Figure 3.12c).

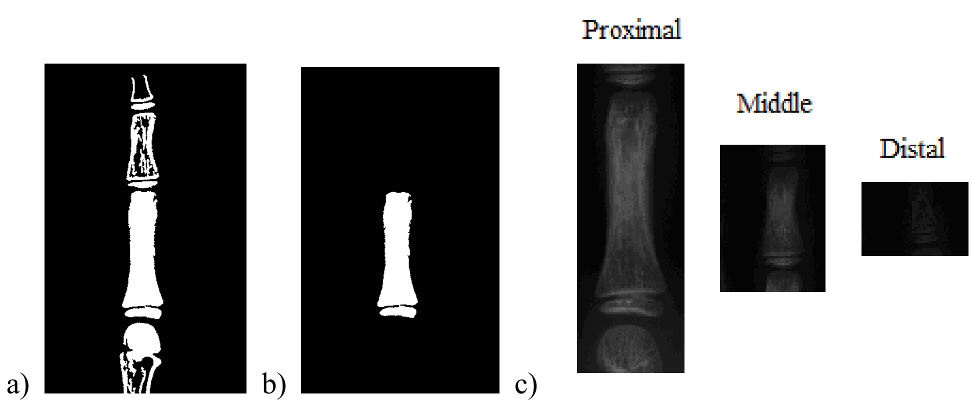

Figure 3.12. Three parts of Phalanx III extraction (step III). a) Binary image of Phalanx III without soft tissue; b) binary mask of the proximal part of Phalanx III; c) segmented proximal, middle and distal parts of Phalanx III.

Very similar operations are implemented for Phalanx I and Phalanx V to obtain the proximal and distal parts of Phalanx I, together with the proximal, middle and distal parts of Phalanx V, which have indicators to be graded in the FELS method. However, there are two things to be noted: First, for the Phalanx III and V ROIs, the selected regions containing the phalanges of interest are the left third of the image for Phalanx V and the right third of the image for Phalanx I instead of the middle region that has been selected for Phalanx III; second, the extracted phalanges of interest need to be rotated first, using the mid line of the bone mask, in order to correctly segment the different parts of the phalanges.

3.3.2 Metacarpals ROIs Extraction

Using the hand-forearm junction line, which was obtained in the orientation correction section (Figure 3.6), together with the bottom line used to extract the phalanges ROI (Figure 3.8), we can also segment the metacarpals ROI by adding a constant number of buffer rows to the top and the bottom (Figure 3.13a). In this region, the first, third and fifth metacarpals need to be extracted separately, since there are FELS indicators to be graded on these specific bones. To achieve this goal, we first apply a range operation on the segmented Metacarpal ROI (Figure 3.13a). The range operator is an adaptive thresholding method, in which each pixel is assigned the value of the difference between the maximum and minimum values within the k x k neighborhood (k = 3 here) (Figure 3.13b).[16] Then the next step is the application of a simple global threshold based on the mean of the range image to obtain the binary image of the metacarpal region (Figure 3.13c). In the resultant image, scanning from the bottom row, a new line is detected where the number of zero crossings first exceeds four (Figure 3.13d).

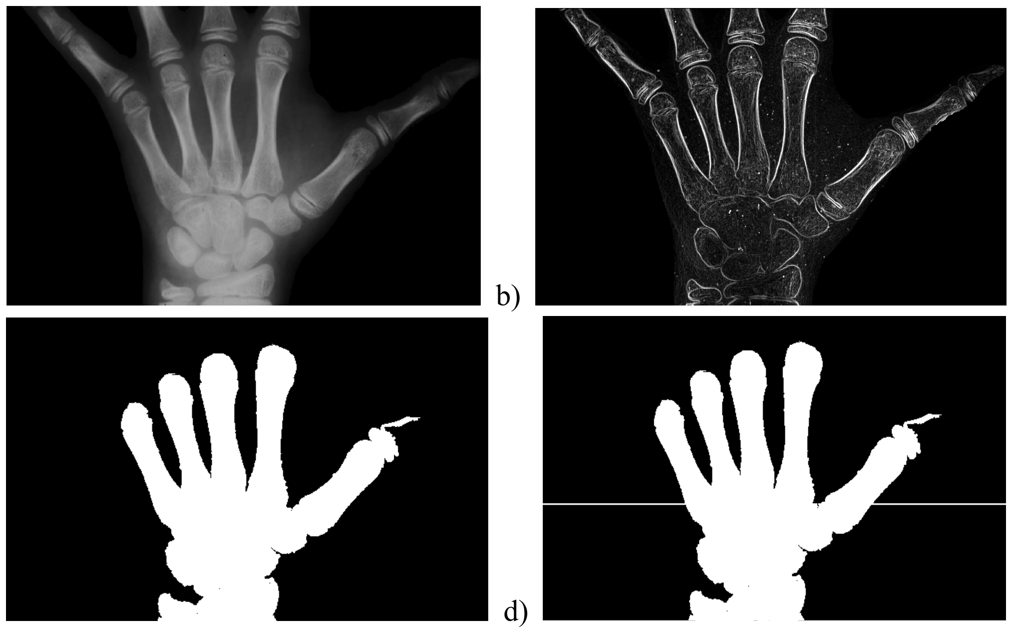

a) b) c) d)

Figure 3.13. Metacarpal segmentation (step I). a) Metacarpal ROI; b) a range operator is implemented on a); c) a global threshold is applied to b) to generate a binary image of a); d) the line where the number of zero crossings first exceeds four.

Also, using the binary mask of the metacarpal ROI (Figure 3.13c), we can get the locations of the tips of the third and fifth metacarpals. Similar to what we did in the phalanx ROI extraction section, the metacarpal tips, together with the line shown in Figure 3.13d, can be used to create a bounding box with a constant width in order to segment the third and fifth metacarpals (Figure 3.14a and b). It should be noted that the proximal end of the third and fifth metacarpals do not have to be included in the extracted region, since there is no indicator to be graded at the proximal end of these two metacarpals. Similarly, using the position of the third zero crossing on the selected line in Figure 14d, we can also create a bounding box to segment the first metacarpal, and the distal end of it does not have to be fully included either.

Figure 3.14. Metacarpal segmentation (step II). a) The third metacarpal; b) the fifth metacarpal; c) the first metacarpal.

3.4 Algorithms of Different Indicators

In the FELS method, the assessment of skeletal age from a radiograph depends upon the recognition of many maturity indicators. The gradings of these indicators are then transformed into a skeletal age by a weighted system. The program to estimate the skeletal age for individuals requires the grading of indicators that should be assessed, and that depends upon the chronological age and sex of the child. The program does not require every indicator to be graded, but, if some indicators appropriate for the age and sex of the child are omitted, the estimated skeletal age will be less precise.

In the FELS method, there are a total of 98 indicators which can be used for the assessment of skeletal maturity, although not all of them need to be graded for each child. These indicators can be generally divided into the following categories: The most commonly used indicators, which need to be recognized for all the long bones of the hand; the relatively commonly used indicators, which require the assessment of size, shape or some other feature of a specific bone; the remaining indicators of different bones. In this section, the description of the different categories of indicators will be presented separately, followed by the algorithms used to grade each kind of indicator.

3.4.1 The Most Commonly Used Indicators

A. Ratio Between the Widths of Epiphysis and Metaphysis

Description

The ratio between the width of the epiphysis and the width of the corresponding metaphysis is one of the most commonly used indicators. It is very useful in normal individuals, since it can precisely reflect the stage of ossification.

To recognize this indicator, we first need to measure the maximum width of the metaphysis at a right angle to the long axis of the corresponding long bone. Then the epiphyseal width is measured as the maximum distance across the epiphysis along a line parallel to the measurement of the metaphyseal width (Figure 3.15). Subsequently the ratio is calculated as:

$$Ratio = \frac{EpiphysealWidth}{MetaphysealWidth}$$

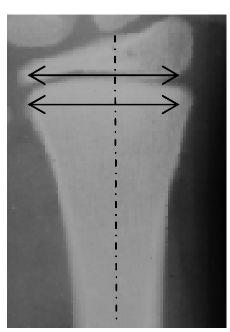

Figure 3.15. Ratio of widths. The lines along which the epiphyseal and metaphyseal widths of the radius are measured for indicator r2.

The age ranges for boys and girls that require the recognition of ratios of each bone are listed in Table 3.1.

Table 3.1. Age ranges for different epiphyseal/metaphyseal width ratio indicators.

INDICATOR	BONE	AGE RANGE	
		Boys	Girls
r2	Radius	0.5 to 12.5 years	0.5 to 12.5 years
u2	Ulna	7.0 to 13.5 years	5.5 to 12.0 years
me12	Metacarpal I	3.5 to 13.0 years	1.5 to 13.0 years
me32	Metacarpal III	3.0 to 13.5 years	2.5 to 13.0 years
me52	Metacarpal V	1.5 to 16.0 years	1.0 to 15.0 years
pp12	Proximal phalanx I	2.5 to 13.0 years	2.5 to 11.0 years
pp32	Proximal phalanx III	2.5 to 11.5 years	2.0 to 12.0 years
pp52	Proximal phalanx V	1.5 to 14.5 years	0.75 to 14.0 years
mp32	Middle phalanx III	1.5 to 13.5 years	0.75 to 12.0 years
mp52	Middle phalanx V	3.5 to 14.0 years	1.0 to 11.0 years
dp12	Distal phalanx I	1.0 to 12.0 years	1.5 to 11.0 years
dp32	Distal phalanx III	2.5 to 10.5 years	1.5 to 20.0 years
dp52	Distal phalanx V	2.5 to 11.0 years	1.5 to 10.5 years

Algorithm

For the ratio indicators, we first need to adjust the contrast of the ROI and create a mask of the bone of interest in the corresponding ROI (Figure 3.16a). All of these steps use the same methods as mentioned in the “Image Classification”, “Background Elimination” and “ROIs Extraction” sections. Next, we use the vertically flipped mask image (Figure 3.16b) to generate a profile showing the number of white points on each row of the image (Figure 3.16c). After smoothing, the first two peaks of this profile should reflect the maximum widths of the metaphysis and epiphysis, respectively. Then, the ratio of them can be calculated.

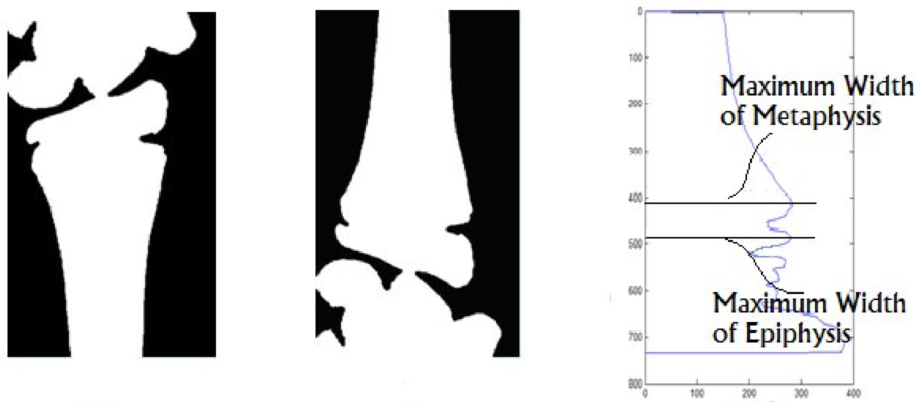

a) b) c)

Figure 3.16. Analysis of indicator r2. a) Mask of radius; b) vertically flipped mask image; c) profile showing the number of white points in each row and the position of the maximum width of metaphysis and epiphysis.

It should be noted that, before generating the profile, we first need to rotate the bone of interest to make its long axis to be vertical, so that the number of white pixels of each row represents the maximum width at right angle to the long axis of that bone. The rotation function uses the midline of the lower one third part of the long bone as a reference line.

If there is only one peak that can be detected in the bone interest region, then the grade of this indictor will be given “0”, which means “not able to be graded”.

B. Epiphyseo-Diaphyseal Fusion

Description

The epiphyseo-diaphyseal fusion is also of considerable importance as a maturity indicator, although it is more difficult to be categorized than the ratio between measurements of bone width. The epiphysis usually ossifies after birth. As age increases, the bony penetration advances from the initial focus (Figure 3.17a) to all directions (Figure 3.17b). Penetration continues until the edges of the metaphysis are reached (Figure 3.17c). The strip between the shaft and the ossification center diminishes progressively (Figure 3.17d) in thickness until it disappears completely at the termination of growth (Figure 3.17e), when the epiphysis and metaphysis fuse into one adult bone. This event is called epiphyseal-metaphyseal fusion.

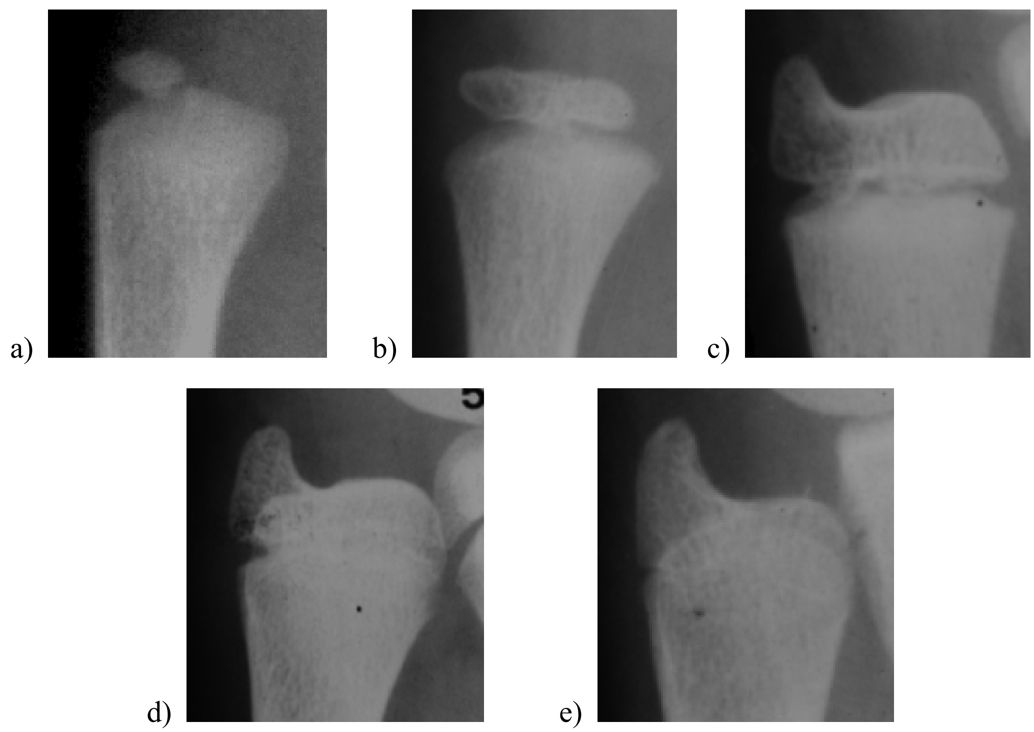

Figure 3.17. Epiphyseal ossification at different stages of development (ulna).

To recognize the fusion of the radius, the FELS method divides the bone in to three parts: medial third, lateral third and central third of the epiphyseo-diaphyseal junction. Indicators R-6 and R-7 represent the capping and fusion of the medial third and lateral third of the epiphyseo-diaphyseal junction, respectively. Indicator R-8 represents the fusion of the central third of that junction. For R-6 and R-7, grade 1 is assigned when capping and fusion are absent in the medial third or the lateral third of the epiphyseo-diaphyseal junction (Figure 3.18a). Grade 2 is assigned when capping is present, but fusion is absent in the two junction regions (Figure 3.18b). “Capping” is recorded as present if the medial or lateral part of the proximal margin of the epiphysis is parallel to the edge on the opposite margin of the metaphysis. Fusion is absent when a relatively radiolucent strip extends the whole length of the medial or lateral third of the epiphyseo-diaphyseal junction. Grade 3 is assigned when capping is present and fusion is incomplete (Figure 3.18c). Incomplete fusion is present when a bony union forms between the epiphysis and the diaphysis across part but not the entire medial or later third of the junction region. At last, grade 4 is assigned when fusion is complete in the medial or lateral third of the junction region (Figure 3.18d). If the fusion is complete, the ratio indicator can not be measured any more and will be given “0”. For R-8, the criteria for absent, incomplete and complete fusion are similar to those for R-6 and R-7, and there are only 3 grades for this indicator, since the “capping” feature is no longer usable for this region.

Figure 3.18. Fusion development (radius). a) Capping and fusion are absent in the epiphyseo-diaphyseal junction; b) capping is present, but fusion is absent in the medial and lateral third of epiphyseo-diaphyseal junction; c) capping is present and fusion is incomplete in the medial third of epiphyseo-diaphyseal junction; d) fusion is complete in the medial and lateral third of epiphyseo-diaphyseal junction.

For fusion indicators that belong to other long bones on the hand/wrist, there are always 3 grades which are the same as those for R-8. The fusion of the ulna is the only one special case that has only 2 grades. For this indicator (U-2), grade 1 is assigned when the epiphyseo-diaphyseal fusion is either absent or incomplete, and grade 2 is assigned when the fusion is complete.

The epiphyseo-diaphyseal fusion is the final phase of skeletal maturation, after which elongation of a bone can not occur. The recognition of it is useful at ages generally older than 11 years. The age ranges for boys and girls that require the recognition of fusion indicators for the various bones are listed in Table 3.2.

Table 3.2. Age ranges for different fusion indicators

INDICATOR	BONE	AGE RANGE	
		Boys	Girls
r6	Medial third of radius	10.0 to 22.0 years	8.5 to 22.0 years
r7	Lateral third of radius	11.0 to 22.0 years	9.0 to 22.0 years
r8	Central third of radius	13.5 to 20.0 years	12.0 to 20.0 years
u3	Ulna	15.5 to 22.0 years	13.5 to 20.0 years
me17	Metacarpal I	13.0 to 20.0 years	10.0 to 20.0 years
me35	Metacarpal III	13.5 to 22.0 years	8.5 to 18.0 years
me55	Metacarpal V	10.5 to 20.0 years	10.0 to 20.0 years
pp15	Proximal phalanx I	13.5 to 20.0 years	10.5 to 16.5 years
pp35	Proximal phalanx III	13.5 to 22.0 years	10.5 to 16.5 years
pp55	Proximal phalanx V	13.0 to 20.0 years	10.5 to 17.5 years
mp35	Middle phalanx III	13.0 to 20.0years	10.5 to 16.5 years
mp55	Middle phalanx V	13.0 to 22.0 years	10.5 to 20.0 years
dp14	Distal phalanx I	12.0 to 18.0 years	10.5 to 15.5 years
dp34	Distal phalax III	13.0 to 20.0 years	10.5 to 17.0 years
dp54	Distal phalanx V	13.0 to 22.0 years	10.0 to 16.5 years

Algorithm

Using the radius as an example, we can easily extract the epiphyseo-diaphyseal junction by knowing the positions of the maximum width of the metaphysis and the epiphysis (Figure 3.19a). A fixed number of rows is added to the top and bottom of that region as a buffer zone to make sure that the whole junction region is extracted. Plotting each column of the epiphyseal-metaphyseal junction image (Figure 3.19a) can help generate a sequence of profiles carrying information about the epiphyseal-metaphyseal fusion. If the fusion is absent in one column, there should be a deep valley in the profile of that column at the location of the epiphyseal-metaphyseal junction (Figure 3.19b). On the other hand, if the fusion is complete, the profile should be steady or has only one peak, reflecting the radiopaque line at the level of the fusion. Counting the columns whose profiles show deep valleys, we can get the number of non-fused columns N_{nf}. The stage of the fusion development can be reflected by different ranges of the percentage of non-fused columns P_{nf}. Here, the percentage is equal to N_{nf} divided by N_{total}; N_{total} represents the total number of columns of the epiphyseal-metaphyseal junction image.

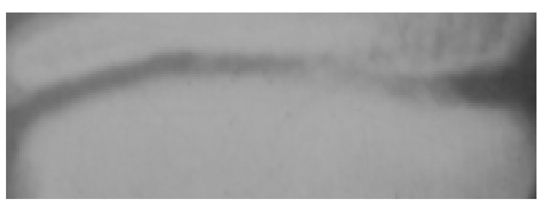

a)

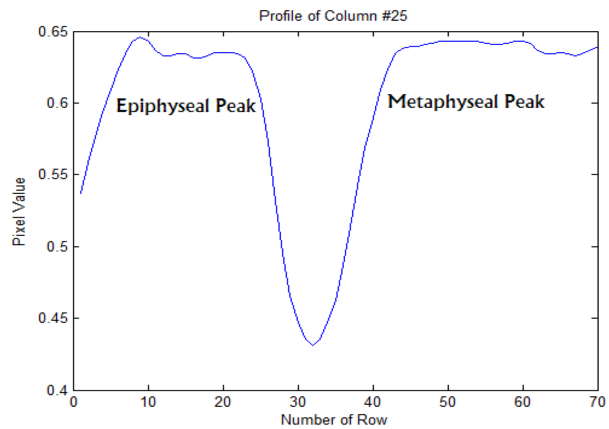

b)

Figure 3.19. Analysis of fusion indicator (step I). a) Region of epiphyseal-metaphyseal junction; b) an example of a profile of a non-fused column in a) (column No. 25).

After careful analysis of the 100 training images in our data base, the relationship between the stage of the fusion development and the range of non-fused column percentages has been established as follows (Table 3):

Table 3.3. Relationship between stage of fusion development and range of $P_{nf.}$

Range of P_{nf}	100% ~ 96%	95% ~ 16%	15% ~ 0
Stage	No Fusion	Incomplete Fusion	Complete Fusion

To analyze the capping feature of the epiphyseo-diaphyseal junction, the locations of the two peaks on the profile of each column are recorded. By calculating the distance between the two peaks (the positions of black pixels in Figure 3.20a), we can establish whether the medial or lateral part of the proximal margin of the epiphysis is parallel to the distal margin of the metaphysis. If the margins are parallel to each other, the distances should be within a specific range, otherwise the “capping” is graded as absent (Figure 3.20b).

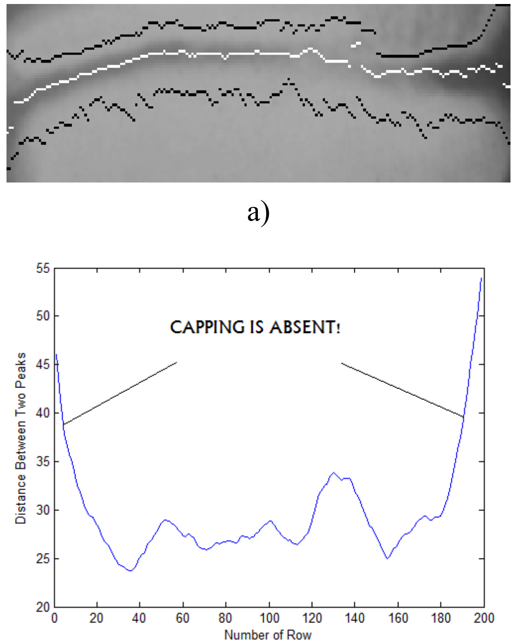

a)

b)

Figure 3.20. Analysis of fusion indicator (step II). a) Epiphyseo-diaphyseal junction with two labeled peaks (black dots) and one valley (white dots) for each column; b) distance between the two peaks of each column.

3.4.2 Relatively Commonly Used Indicators

A. Radiopaque Line Within the Bone

Description

Radiopaque lines within the epiphyseal shadow of the bones on the hand/wrist are relatively commonly used indicators. As the skeleton becomes mature, the margin of the surface of the epiphysis (distal margin of radius, lateral margin of metacarpals and proximal margin of different parts of the phalanges) causes a thick white radiopaque line within the epiphyseal shadow.

With increasing age, this white line extends laterally from the medial margin of the epiphysis for the radius, and it finally reaches the lateral margin. Therefore, the recognition of a radiopaque line **on or within** the distal margin of the epiphysis of the radius is used as one indicator (Figure 3.21a). For Metacarpal III and V, a radiopaque line or zone **within** the lateral margin of the epiphysis should be recognized as an indicator (Figure 3.21b). For the proximal part of Phalanx I, III and V, this radiopaque line or zone should be **within** the epiphyseal shadow, **not on** its proximal margin, but the ends of the line or zone may meet the proximal margin (Figure 3.21c). For the middle and distal parts of Phalanx III and V, a central projection is used as an indicator instead. This projection of the proximal margin of the epiphysis beyond the radiopaque line or zone is due to the dorsal edge of the epiphysis; it is actually the palmar margin of the epiphysis (Figure 3.21d).

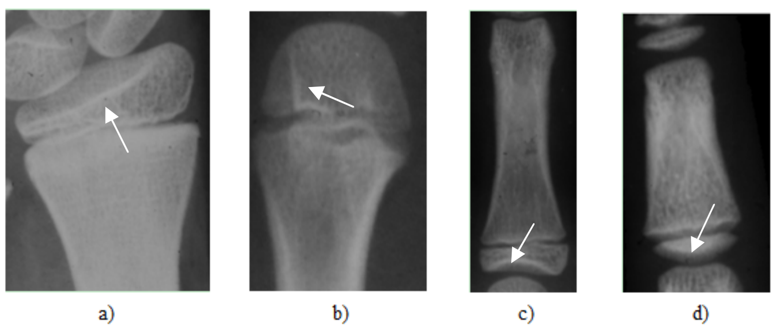

Figure 3.21 Indicators related to radiopaque lines on or within the epiphysis of radius (a), metacarpal (b), proximal phalanx III (c) and middle phalanx V (d).

There are always two grades for this kind of indicator. Grade 1 is assigned when the radiopaque line or projection is absent, and grade 2 is assigned when the radiopaque line or projection can be recognized at the specific location of the epiphysis of the different bones. It should be noted that the indicators related to the radiopaque line of the proximal, middle and distal phalanges are not assessed after the epiphyseo-diaphyseal fusion of these bones is complete. The age ranges for boys and girls that require the recognition of the radiopaque lines for the various bones are listed in Table 3.4.

Table 3.4. Age ranges for different radiopaque line indicators

INDICATOR	BONE	AGE RANGE	
		Boys	Girls
r4	Distal margin of radius epiphysis	0.5 to 8.0 years	0.75 to 6.0 years
me33	Lateral margin of Metacarpal III epiphysis	5.5 to 22.0 years	6.0 to 15.0 years
me53	Lateral margin of Metacarpal V epiphysis	7.5 to 15.5 years	5.0 to 13.0 years
pp14	Proximal margin of Proximal Phalanx I epiphysis	6.5 to 16.5 years	4.0 to 14.0 years
pp34	Proximal margin of Proximal Phalanx III epiphysis	6.0 to 14.0 years	4.0 to 14.5 years
pp54	Proximal margin of Proximal Phalanx V epiphysis	8.0 to 16.5 years	7.0 to 14.5 years
mp33	Epiphysis of Middle Phalanx III	1.5 to 10.5 years	1.5 to 10.5 years
mp53	Epiphysis of Middle Phalanx V	2.5 to 10.0 years	1.5 to 8.5 years
dp33	Epiphysis of Distal Phalanx III	2.5 to 13.0 years	2.0 to 11.5 years
dp53	Epiphysis of Distal Phalanx V	3.5 to 13.5 years	3.0 to 12.0 years

Algorithm

Using the proximal part of Phalanx III as an example (Figure 3.22a), the epiphysis can be easily extracted (Figure 3.22b), since the location of the epiphyseal-metaphyseal junction has been detected when we graded the fusion indicator of Proximal Phalanx III. Furthermore, the position of the maximum width of the epiphysis was also recorded when we graded the ratio between the widths of epiphysis and metaphysis.

Since we are only interested in the proximal margin of the epiphysis, we use the position of the maximum width of the epiphysis to extract the ROI (Figure 3.22c). Then, the Matlab edge-detection function is used to recognize the radiopaque line. This function can identify the places in the image where the intensity changes rapidly, and it returns a binary image containing ones where edges are found and zeros elsewhere. In this project, we use the most powerful edge-detection method – the Canny method [18] to identify the edge. This method uses two different thresholds (to detect strong and weak edges), and includes the weak edges in the output only if they are connected to strong edges. This method is therefore less likely than the others to be fooled by noise and more likely to detect true weak edges (Figure 3.22d).

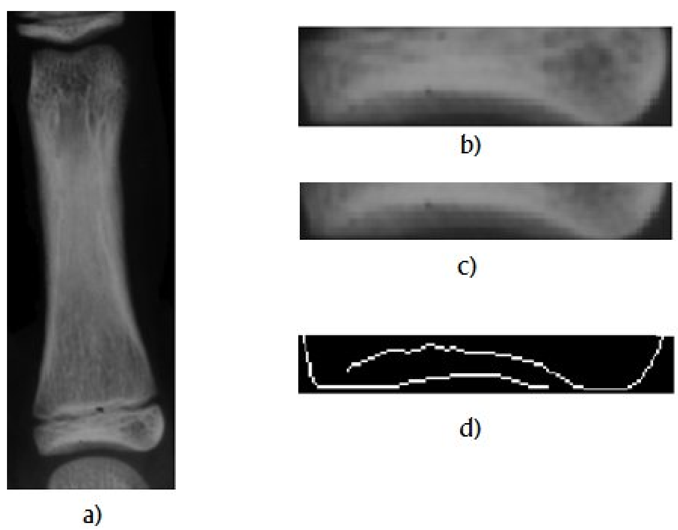

Figure 3.22. Analysis of indicator pp34. a) Proximal Phalanx III; b) epiphysis of Phalanx III; c) proximal margin ROI of the epiphysis of Proximal Phalanx III; d) binary image after edge detection of c).

After edge detection, the number of columns N_c that contain more than one white pixel is counted. Since the edge-detection function always returns a one-pixel wide edge, more than one white pixel means that there are two edges can be detected in that column. These two edges reflect the presence of the radiopaque line. If N_c is greater than half of the maximum width of the epiphysis, it means that a radiopaque line or zone is present on the margin, and grade 2 is assigned. Otherwise grade 1 is assigned, indicating that the radiopaque line is absent.

B. Shape of Bones

Description

In the FELS method, another relatively commonly used indicator is the shape of the bones in a hand/wrist radiograph. The proximal margin of the epiphysis of proximal phalanx I, III and V fall into this category. The usual age progression in the shape of the proximal margin of the epiphysis of these bones is from convex to flat to concave. Therefore, in specific age ranges, these margins can be used as important indicators to help assess the bone maturity. In these cases, grade 1 is assigned when the proximal margin of the epiphysis is not concave (Figure 3.23a and b), and grade 2 is assigned when the margin is concave (Figure 3.23c). These indicators are not assessed after the epiphyseal-diaphyseal fusion is complete.

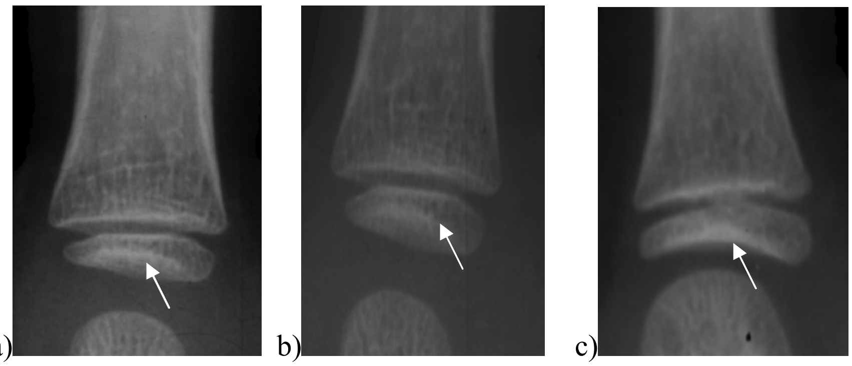

a) b) c)

Figure 3.23. Indicators related to the shape of the proximal margin of the epiphysis. Examples of grade 1 -- (a) and (b) and grade 2 -- (c) of the concavity shape indicator at the proximal margin of the epiphysis.

The age ranges for boys and girls that require the grading of the proximal margin of the epiphysis of specific bones are listed in Table 3.5.

Table 3.5. Age ranges for grading the proximal margin of the epiphysis of different bones.

INDICATOR	BONE	AGE RANGE	
		Boys	Girls
pp13	Proximal phalanx I	1.5 to 10.0 years	1.0 to 10.0 years
pp33	Proximal phalanx III	0.5 to 8.0 years	0.5 to 7.0 years
pp53	Proximal phalanx V	0.75 to 9.0 years	1.0 to 7.0 years

Another kind of shape that falls into this category is the distal end of the proximal and middle phalanx I, III and V. For these bones, grade 1 is assigned when the margin is round or flat (Figure 3.24a); grade 2 is assigned when it is concave (Figure 3.24b).

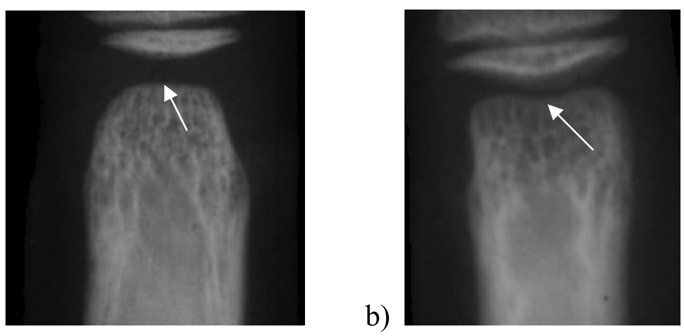

a) b)

Figure 3.24. Indicators related to the shape of the distal end of the proximal phalanges. Examples of grade 1 (a) and grade 2 (b) of indicators regarding the shape of the margin of the distal end of the proximal phalanges.

The age ranges for boys and girls that require the grading of the distal end of specific bones are listed in Table 3.6.

Algorithm

In order to recognize the shape of bones, the edge-detection function that we used to grade the radiopaque lines can also be used here. Once we get the edge of the region of interest (Figure 3.25a and b), the row number of the white pixel in each column is saved in a vector *x* (Figure 3.25c), and the vector *x* is smoothed to remove noisy peaks.

Table 3.6. Age ranges for grading the distal end of different bones.

INDICATOR	BONE	AGE RANGE	
		Boys	Girls
pp16	Proximal phalanx I	5.5 to 15.0 years	3.5 to 12.5 years
pp36	Proximal phalanx III	2.5 to 14.5 years	0.75 to 11.5 years
mp34	Middle phalanx III	7.5 to 22.0 years	5.0 to 15.5 years
mp54	Middle phalanx V	8.5 to 22.0 years	8.0 to 22.0 years

Then, a Matlab built-in function *[pks, locs] = findpeaks(x)* is applied to find local maxima or peaks in vector *x*. This function compares each value in *x* with its neighboring values; if a value is larger than both of its neighbors, it is a local peak, and its location is returned in the vector *locs*. Consequently, if two peaks can be detected and their locations are relatively far away from each other, the shape of the region of interest is concave.

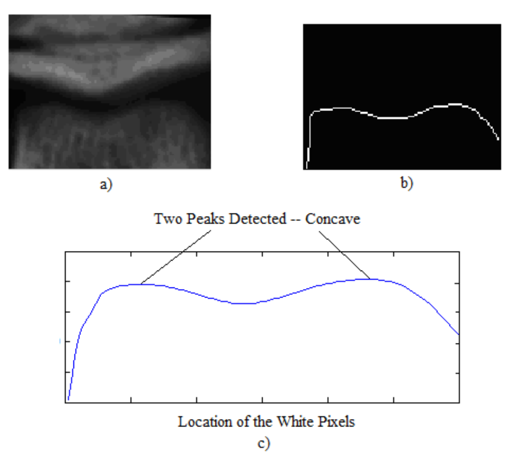

Figure 3.25. Analysis of the shape indicators. a) The region of interest (distal end of proximal phalanx III); b) edge of the distal end; c) plot of smoothed vector containing the row number of white pixels in each column of b).

3.5 Analysis of DXA Images

Dual x-ray absorptiometry (DXA) is a newer technique for measuring bone-mineral density. DXA is relatively easy to perform, and the amount of radiation exposure is lower than that of a normal radiograph.[19] The DXA scanner used for our measurements produces two x-ray beams (separated in time), each with a different energy. The intensity of the x-rays that pass through the patient is measured for each beam. This intensity will vary depending on the thickness of the bone and the soft tissue. Based on the difference between the two beam intensities, the amount of bone can be measured.[19]

DXA is the most widely used and thoroughly studied bone density measurement technology.[20] It is, therefore, of interest to find out if the image quality of DXA is sufficient to assess the skeletal age of children. The low radiation exposure associated with DXA would be a major advantage in the use of this technology.

In order to evaluate the suitability of DXA for bone age assessment, a DXA left hand/wrist image was taken with DXA scanner model QDR 4500 Discovery A at the same time when each child from the Fels Longitudinal Study underwent the traditional radiograph hand/wrist procedure. A special Plexiglas holder was built to allow reproducible positioning of the hand in the relatively narrow field of view. The DXA images were first adjusted in the Hologic Apex Software to produce a good-quality gray-level presentation; the reports were then saved as de-identified DICOM files for later processing (Figure 3.26a). The grayscale resolution of these

DXA images was 8-bit, and the spatial resolution was 500 μm per pixel.

a) b)

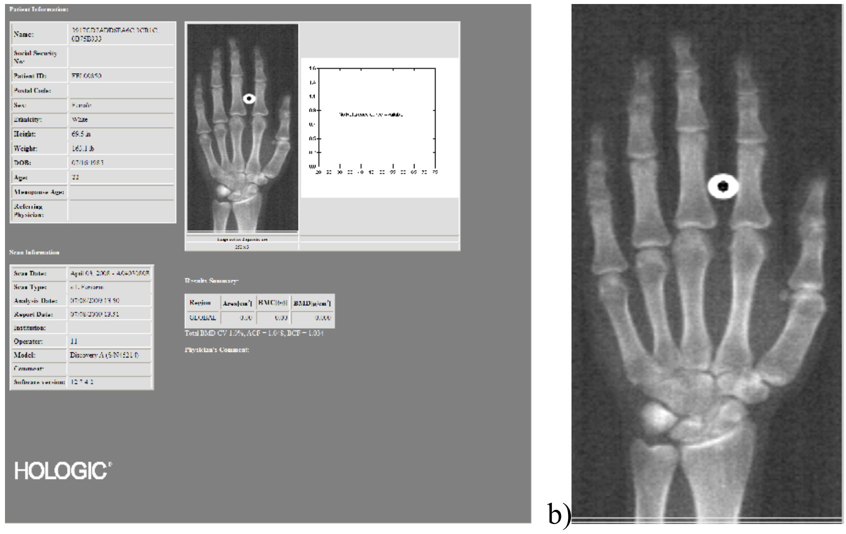

Figure 3.26. DXA image. a) Interface of the software used to analyze DXA images; b) extracted DXA image.

The DICOM file contains the image and additional patient and analysis information. The first processing step consisted in extracting the image region and saving it as a Tiff file (Figure 3.26b). Since the DXA image region is always at a consistent location, it was easy to extract this region automatically. Next, background estimation (Figure 3.27b) and suppression (Figure 3.27c), which was described in section 3.2.2, is performed on the original extracted image (Figure 3.27a) as part of image preprocessing.

a) b) c)

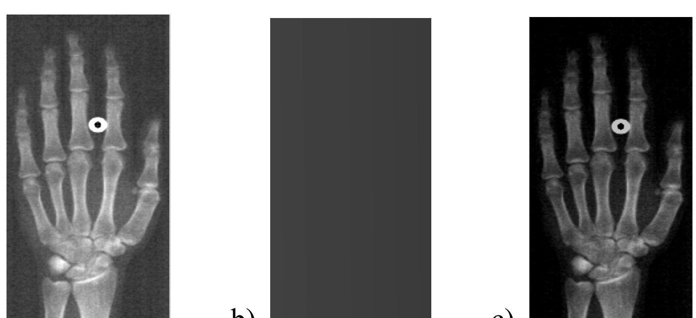

Figure 3.27. Background estimation and suppression of DXA image. a) Original DXA image; b) background estimation of a); c) background suppression of a).

The extraction of interested bones on the left hand/wrist is still based on thresholding. An optimal threshold value is automatically set based on Otsu's method by using Matlab's *graythresh* function, and a binary image is obtained (Figure 3.28a). Then, the same method used for normal x-ray images is applied to locate the hand-forearm junction and tips of the first, third and fifth phalanges. The difference is that the proximal end of the first, third and fifth phalanges are located using the position of the white circle object with a black centre between the second and third phalanges. This object was used to ensure standard orientation of the hand/wrist, so there is no need to perform the orientation correction for the DXA images. Since this object always appears as a white circle on the original DXA image (Figure 3.27a), we first threshold the image using a gray value of "1" (which means white) and then remove the possible parts of bones to get this object. Since the possible parts of bones are just small objects comparing with the white circle, the "bwareaopen" function in Matlab can be used to remove them. This function works as morphologically opening binary image. It removes all connected components (objects) that have less than a defined number of pixels from a binary image. Once the white object is recognized, fixed numbers of rows are added to the location of the object in order to identify the approximate region of the proximal end of the first, third and fifth phalanges.

To extract the metacarpals, the junction of the first and second metacarpal can be detected by counting the zero crossings on each row on the mask (Figure 3.28c). This method was also described in section 3.3.2. This line can be used to get the proximal end of the first, third and fifth metacarpals.

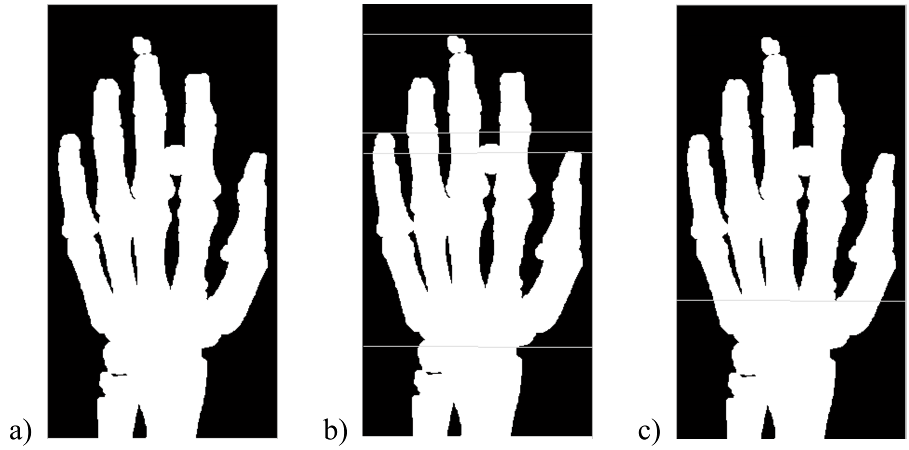

Figure 3.28. Bones identification of DXA image. a) Binary image of Figure 28c; b) locations of the tips of the 1st, 3rd and 5th phalanges and the hand-forearm junction; c) location of the junction between the 1st and 2nd metacarpals.

Once we have identified all of the bones of interest, the algorithms of grading different indicators are almost the same as those for the traditional x-ray images. However, the feature recognition functions, especially the ones based on the edge detection algorithm, are highly affected by the poorer spatial resolution of the DXA images compared to the traditional images (500 μm per pixel vs. 85 μm per pixel).

Chapter 4

Result and Discussion

After applying a variety of image processing algorithms to extract the quantitative features associated with the different indicators of the left hand/wrist radiographs, all the grades assigned to a specific patient are recorded in an Excel spread sheet as one column in a predetermined sequence. Then the user needs to manually input the child's chronological age and sex of that patient at the bottom end of the column.

This Excel file is then run through a computer program to calculate the skeletal age. The program attempts to assess all indicators of the FELS method, even those that are not necessary to be assessed for patients at a specific age. The aim of doing this is to make the program usable even if the chronological age of a child is unknown. By knowing the chronological age of a child, the unnecessary indicators are given a reasonable grade by default, usually the highest grade in our study. This is due to the fact that these missing indicators are used for children from newborn to 7 years old, and for the age range in our study, the features related to these indicators have already matured.

The grades assigned to a radiograph together with the information of the patient are saved in a TXT file (Appendix I). The TXT files generated from each of the data sets are merged into one TXT file using a small program written in BASIC. This file is then imported to a program written in PASCAL, which was developed by researchers at the Lifespan Health Research Center. This program helps to calculate an estimated skeletal age and a standard error of each participant; it also saves all the participants' results in an Excel spread sheet for further analysis. The standard error calculated by this program is provided by the FELS method for the assessment of skeletal maturity. It is a measure of the confidence limits of a specific age due to the variability of the age relationship of the various indicators. The confidence limits establish the range of values, within which the true, but generally unknown, skeletal age lies.[11]

4.1 Success of Automated Preprocessing Analysis

In this study, 174 traditional x-ray images (100 for training and 74 for testing) and 74 DXA images (all for training) were used to evaluate the success of the automated preprocessing algorithm. The preprocessing analysis can be divided into several steps to evaluate the success:

1) Background Removal and Hand Segmentation

In this step, background estimation and suppression are performed, and the hand is extracted by suppressing the nonuniform background with a mask of the hand. A total of 7 images of the training set and 4 images of the testing set failed this step. The failure was generally due to the poor quality of the image (Figure 4.1a and b). In the

DXA image set, all of the 74 images successfully run through the first step and were able to generate a mask of the bones.

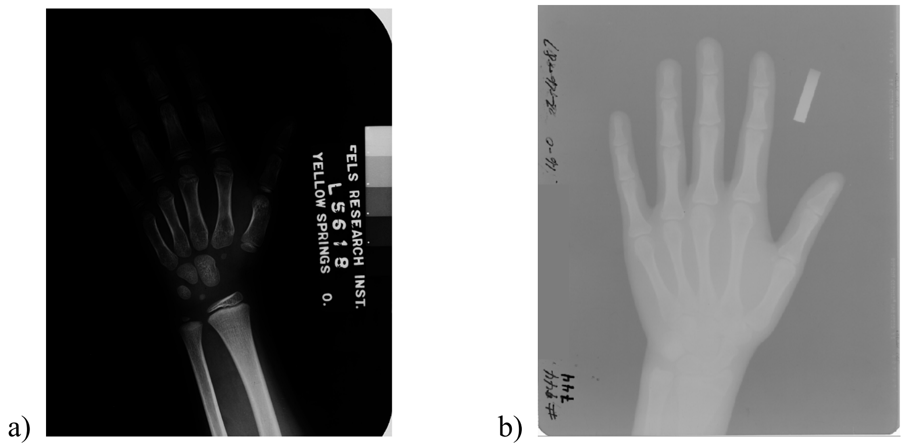

Figure 4.1. Images with poor quality, which are failed the background removal step.

2) Orientation Correction

In this step, two types of images are of concern. Depending on whether an angle exists between hand and forearm, there are two procedures to be implemented. First, in the procedure of the image rotation based on the midline of the forearm, one image of the training set and two images of the testing set failed to be correctly rotated. Second, in the procedure of the image rotation based on the connection of the tip of the third phalanx and the mid point of the line at the hand-forearm junction, all of the training images were successfully rotated to the standard orientation, but one image of the testing set failed. The failures in the two procedures of the orientation correction step were due to high degrees of hand rotation in the original images. In these cases only a short forearm part could be used to set the reference line, or the highest positioned white point of the hand mask represented the fourth or fifth phalanx and not the tip of the third phalanx. For the DXA image set, since a special Plexiglas holder was used to allow reproducible positioning of the hand in the relatively narrow field of view, the images were all at the standard orientation and did not need to be rotated.

3) Localization of Bones of Interest.

In the step of identifying all the bones that need to be graded in the FELS method, there were 2 images in the training set with one or two bones that were not extracted accurately. For the testing set, 4 images had similar problems. All of the DXA images were successful in the localization of the bones of interest due to the fact that the hands were all scanned in a reproducible position.

In order to clearly show the statistical result of the success of the preprocessing steps, the number of failures in each step and the percentages are listed in Table 4.1. Compared to the radiographs, the DXA set shows very good performance in the preprocessing steps. The low resolution of the DXA images appears not to influence the success of the segmentation step. After the preprocessing stage, all of the bones of interest are correctly extracted for the following analysis. All images making it successfully through the preprocessing steps can be analyzed with respect to the various indicators, and none of them fails in the later steps. For the images that failed in the preprocessing steps, manual intervention -- normally the ROI localization -- allows them to be analyzed by the later steps, but some of them fail again in those steps. The cases that failed in any preprocessing step were dropped from the totals and are not included in our later statistics.

Table 4.1. The number of successes and the percentage of successes in each preprocessing step.

	Training Set	Testing Set	DXA Set
Background Removal & Hand Segmentation	93 (out of 100, 93%)	70 (out of 74, 94.6%)	74 (100%)
Orrientation Correction	93 (out of 93, 99%)	67 (out of 70, 95.7%)	74 (100%)
Localization of Bones of Interest	90(out of 92, 97.8%)	63 (out of 67, 94%)	74 (100%)
Total	90 (out of 100, 90%)	63 (out of 74, 85%)	74 (100%)

4.2 Comparison of Manual vs. Automated Analysis

Accuracy of Each Indicator

To test the performance of the grading system, we recorded the grades of all indicators, which were assessed from the images that successfully passed the preprocessing steps. The same images were also analyzed by two well trained image analysts at the Lifespan Health Research Center. The grades provided by these two analysts, after they reached consensus and one grade of each indicator was provided, were used as reference values (most of the time, these two specialists provided identical opinions). In the training set, we have 90 observations for each indicator generated from the automated analysis method to be compared with the reference values (10 out of 100 failed in the preprocessing steps). In the testing set we have 63 observations of each indicator (11 out of 74 failed in the preprocessing steps), and in the DXA image set we have 74.

To test the hypothesis that there is no significant difference between our observation and the reference value (p-value = 0.05), the following equations were used for each indicator in the training set, testing set and DXA image set separately:

$$\Delta_i = O_i - R_i \qquad (4.1) \qquad\qquad Mean = \frac{\sum_{i=1}^{n} \Delta_i}{n} \qquad (4.2)$$

$$SD_{\Delta} = \sqrt{\frac{\sum_{i=1}^{n} (\Delta_i - Mean)^2}{n-1}} \qquad (4.3) \qquad\qquad SD_{Mean} = \frac{SD_{\Delta}}{\sqrt{n}} \qquad (4.4)$$

where, O is the observation value of each indicator, R the reference value, i the different individuals, Δ the difference between the observation and reference value of each individual and n the number of the observation values that are not equal to zero. It should be noted that n is always less than the total number of observations we analyzed by our program. When the specialists assigned zero (which means unable or unnecessary to be graded) to a specific indicator for an individual, our observation value was corrected to zero and is not included in the comparison. This is due to the fact that the program tries to analyze all of the indicators, but for each individual, there are a number of indicators unnecessary to be graded. For example, when the epiphysis and metaphysis of metacarpal III have been fused, the shape of the epiphysis does not need to be graded. Or it may be difficult to grade them even by a specialist's visual assessment. Sometimes the feature of an indicator is unusable in a radiograph; for example, part of the distal end of phalanx I is not covered in the field. This kind of assessment can easily to be made by a specialist but not by the program.

If the observation values of these indicators are included in the comparison, the accuracy of our program will be highly affected.

After getting the mean (Equation 4.2) and standard deviation of the mean (Equation 4.4), we generated a plot of all indicators (Figure 4.2 a, b and c) for each data set. This plot shows the *Mean* and *Mean* ± 2 SD_{Mean} of each indicator, except for the indicators that belong to the carpal bones, which were not analyzed in our study.

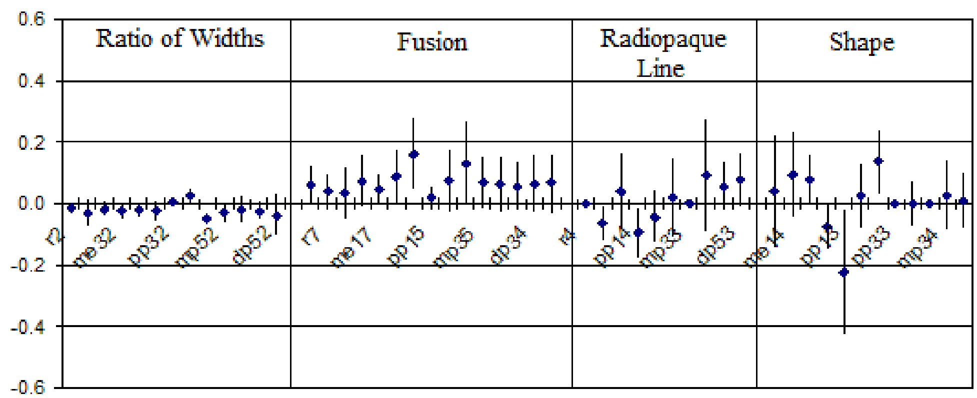

(a)

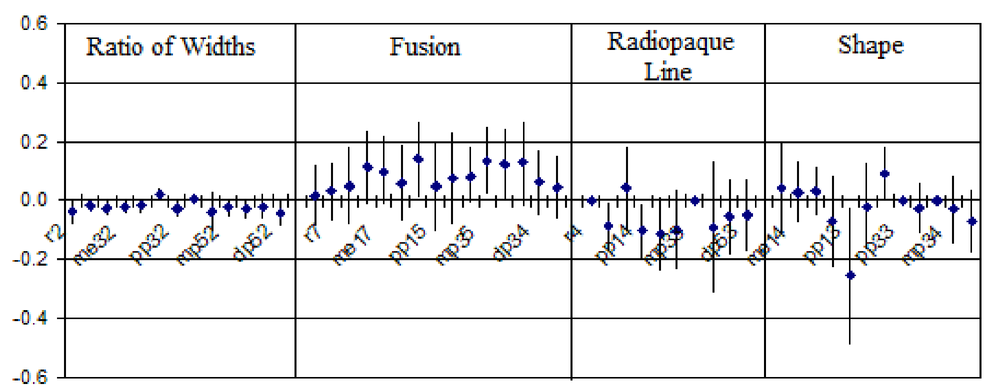

(b)

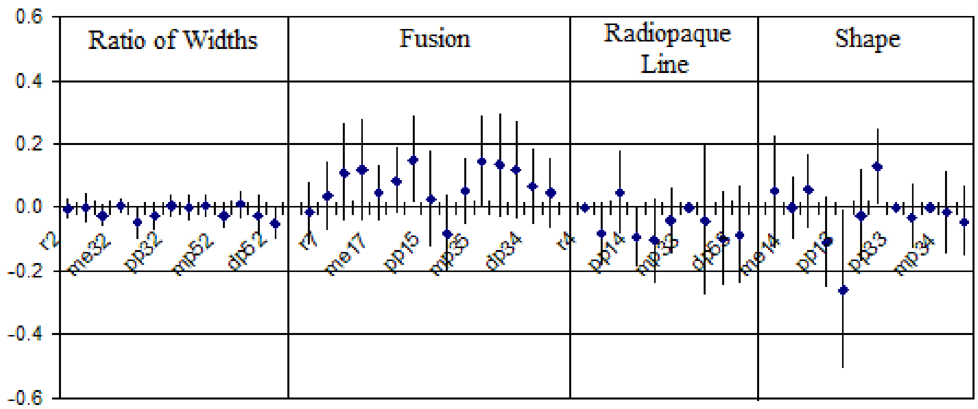

(c)

Figure 4.2. Plot of *Mean* and *Mean* ± 2 SD_{Mean} of each indicator from a) training set; b) testing set; c) DXA set.

From these plots, we can test our hypothesis by checking whether the range of *Mean* ± 2 SD_{Mean} includes the zero value. If the range does not include zero, the null hypothesis will be rejected. We find that, for the indicators me16, me33, me55, me56, pp13, pp14, pp17 and mp32 of the training set, me33, me55, pp13, pp14, pp17, mp35, me12 and pp12 of the testing set and me55, pp13, pp14, pp17, mp35 and dp52 of the DXA set (Table 4.2), the values obtained from the automated analysis method show significant differences compared with the reference values (Appendix II). In general, most *Means* of indicators are closer to zero in the training set than those in the testing and DXA sets, which means that the training set achieved better agreement with the experts.

We can find that among the 12 low-accuracy indicators, 3 of them (me16, me55 and me35) are related to the fusion region of metacarpals, and another 2 (me33 and me56) concern the shape of the epiphysis of metacarpals. The results are influenced by overlapping of epiphysis and metaphysis of these bones. This overlapping might obscure both the disto-medial corner of the epiphysis and the radiopaque line.

Table 4.2. Indicators with low accuracy

Indicator	Description
me16	Medial capping of the distal margin of the epiphysis
me33	Radiopaque line or zone within the lateral margin of the epiphysis of metacarpal III
me55	Epiphyseo-diaphyseal fusion of metacarpal V
me56	Indentation of the medial margin of the epiphysis of metacarpal V
pp13	Proximal margin of the epiphysis of proximal phalanx I is concave.
pp14	Radiopaque line or zone within the proximal margin of the epiphysis of proximal phalanx I
pp17	Disto-medial projection of the epiphysis of proximal phalanx I
mp35	Epiphyseo-diaphyseal fusion of middle phalanx III
mp32	Epiphyseal width / metaphyseal width for middle phalanx III
me12	Epiphyseal width / metaphyseal width for metacarpal III
pp12	Epiphyseal width / metaphyseal width for proximal phalanx I
dp52	Epiphyseal width / metaphyseal width for distal phalanx V

Another reason that might affect the result is the larger soft-tissue thickness in the palm region. If we consider the soft tissue as the background of the ROIs, the nonuniform background may lead to failure in thresholding. Even the function we used to remove the soft tissue does not work in some cases. Therefore, part of the ROI might not be extracted correctly. There are also 3 indicators concerning features of the epiphysis of proximal phalanx I, especially the proximal margin. The accuracy of these indicators is also influenced by the soft tissue in this region. Some indicators related to the ratio of the epiphysis and metaphysis widths also show low accuracy, which might be caused by inaccurate thresholding.

Accuracy of the Skeletal Age Assessment

After testing the accuracy of each individual indicator, we integrated all indicators and tried to test three issues:

1) Whether the final output, skeletal age, is impacted by these low-accuracy indicators.

2) Whether the significance level we defined for the hypothesis about the validity of each indicator is reliable.

3) Whether the indicators that the program failed to grade (which were assigned "0" by default) highly influenced the final result.

In order to answer these questions, first, the grades of all the indicators of the participants that were generated by the automated system were recorded as TXT files and run through the PASCAL program, which gives estimates of the skeletal age of the participants. The same program was also used to provide age estimations based on the specialists' visual grading. By comparing the skeletal age assessed by our system and that assessed by the specialists, we found that for all the images that can successfully run through the preprocessing steps, 13.3% of the training set, 20.6% of the testing set and 40.5% of the DXA set show large differences (more than one year).

The DXA images show larger differences because the low resolution of the image highly affects the ROI extraction in the indicator analysis part. It should also be noted that the larger differences always pertain to the age range of 13 to 15 years, when the partial fusion of long bones happens. In addition, in the age range of 8 to 10 years, larger differences also arise if the skeletal development of the child is much slower than usual.

We also used two more methods related to the standard deviation provided by the PASCAL program to compare the observation and reference values. The first method was the one we used in testing the accuracy of individual indicators. The difference between the observation value and the reference value was compared with 2 SD_{diff} :

$$SD_{diff} = 2\sqrt{SD_{Ref}{}^2 + SD_{Obs}{}^2} \qquad (4.5)$$

If the difference falls into the range from -2 SD_{diff} to 2 SD_{diff}, the null hypothesis that "there is no significant difference between the observation and reference value" is true. Based on this test, we found that 15.5% of the training set, 25.4% of the testing set and 42% of the DXA set show significant differences. The second method was testing whether the observation value falls into the range of $Ref \pm 2\ SD_{Ref}$ (Ref and SD_{Ref} were estimated by the PASCAL program based on the specialists' visual grading). In this test, we found that 33.3% of the training set, 36.5% of the testing set and 55.4% of the DXA set show observation values outside the range of $Ref \pm 2\ SD_{Ref}$.

Next, in order to test the influence of the ungraded indicators, we manually set the specialists' grades to "0", if the grades of specific indicators were assigned "0" by our program. In this case, better results were obtained: Only 7.7% of the training set, 15.6% of the testing set and 35.1% of the DXA set show large differences (more than one year).

Based on the comparisons we did as mentioned above, we can draw two conclusions: First, the accuracy of the indicators that were successfully graded by our program is fairly good; second, the indicators that were not graded by our program (most of which are the features of the carpal bones) do have some effect on the skeletal age assessment of children 8 to 18 years old, because when we removed the effect of these indicator by setting them to the grades provided by the specialists, better result were achieved. However, at this point, it is hard to say whether this automated method is reliable enough for clinical application.

4.3 Computation Time

The time required to automatically analyze each image varies from 1.5 minutes to 4 minutes. It highly depends on the orientation correction step. If the original image has a standard orientation of the hand/wrist, it is not necessary to rotate the image; therefore some time is saved. On the other hand, if a high degree of hand/wrist rotation presents in the original image, or, even worse, if also an angle exists between hand and forearm, more time is needed to perform the rotation.

In addition, the images used in this study were digitized at 16-bits. Such high grayscale resolution makes the algorithms involving histogram analysis relatively time consuming. One possible solution for reducing the speed of execution of this analysis is using a lower grayscale bit depth, as long as a consistent accuracy of the method can be ensured. Further more, if a standard orientation of the left hand/wrist can be guaranteed when the radiographs are generated, the orientation-correction step will be unnecessary, and the efficiency will be highly improved.

Chapter 5

Conclusion

It is commonly agreed that the FELS method produces estimates of skeletal maturity that are usually more accurate than other widely used methods.[5] This is mainly due to the fact that the FELS method assesses the skeletal maturity based on the features of a total of 22 bones and 98 indicators. Therefore, the set of maturity indicators obtained from these bones provides an accurate representation of the growth process, which allows people to deal with variabilities in the maturation stages of the various bones. Unfortunately, this is also the source of the major limitation of this method. For each examination, the operator has to carefully classify a large number of bones with long execution time. In addition, in order to precisely assess the bone maturity indicators, a specialist with considerable experience is needed to produce accurate result. Thus, automation of the FELS method is highly desirable. It would allow a much more extended use of the method and more accurate clinical examinations.

In this study, we have developed an automatic computer-based analysis tool to establish skeletal age based on the FELS method. This tool was applied to images obtained through the traditional x-ray procedure and also to images obtained from a DXA scanner. Testing the software on a set of 174 traditional x-ray images and 74 DXA images revealed that the program was successful in automatically analyzing images about 85% of the time with no manual intervention. The remaining images were classified by the analyst as being of poor quality. In this group, 61.5% of the images can be successfully analyzed by user intervention. The user intervention includes manually rotating the hand position and extracting bones of interest. The remaining 38.5% could not be analyzed. Therefore, we can conclude that the program is largely independent of user intervention.

By comparing the skeletal age of each participant generated from our analysis method with the reference values provided by specialists at the Lifespan Health Research Center, it was found that the analysis of the traditional x-ray images was fairly good; only 13.3% of the training set and 20.6% of the testing set show differences that are larger than one year. However, the results of the DXA images were worse -- about 40.5% of this data set show a difference larger than one year.

Several automated skeletal age assessment methods have been described in the literature, although none of them was based on the FELS method. For example, Chang CH and Hsieh CW[21] developed a fully automatic computerized bone-age assessment procedure based on ossification analysis of the phalanges. The participants in their study were from 0.5 to 18 years old. A back propagation neural network was used to train the feature analysis, which included the physiological features of the medius and the morphological features of the joint between the distal and middle phalanges. In their study, an error within 1.5 years of age was ignored, and the accuracy of their method was 77.7% by using physiological features and 81.5% by using morphological features. The percentage of images that succeeded in the preprocessing steps was 89.9%.

The accuracy of our method applied to traditional images is better than theirs: only 9.5% of the images of the training set and 12.5% of those of the testing set show differences that are larger than 1.5 years. However, the correct rate of segmentation of our method is somewhat poorer than theirs: about 15% of the images need manual intervention. This is because the quality of the images in our data set was rather variable.

5.1 Challenges in Automated Image Analysis

Thresholding Issues

Automatic threshholding, which is used to first segment the hand and then the bones of interest, is challenging because of large image variability. Differences in anatomy and degree of mineralization across the age range of the Fels participants impact image contrast. Additionally, variability due to film quality also affects the success of our automated routines. We attempted to mitigate the issues related to image quality by customization of the pre-processing steps based on a particular image's overall contrast. However, even after applying appropriate pre-processing steps, the variable film quality was sometimes still an important factor leading to failure in thresholding. In overexposed radiographs, the threshold value obtained from Otsu's method (which relies on the image histogram) tends to remove parts of the hand bones, whereas in underexposed radiographs unwanted background regions are included after segmentation.

Since the algorithm is divided into steps, and each step depends on the success of the previous one, failure at any step is propagated and usually leads to failure of the subsequent steps.

ROI Extraction

Hand anatomy also plays an important role in ROI extraction. The anatomy is variable across the participant’s lifespan. For example, at an early age, the metacarpals and carpals are well separated, but over time they begin to overlap, and distinguishing the boundaries is impossible at times. There is a total of 7 indicators related to the proximal end of the first metacarpal. Analysis of these indicators is therefore sometimes not accurate when this bone overlaps with carpals.

Furthermore, there are 31 indicators referring to carpal bones in the FELS method. These indicators were not analyzed in our study, because our analysis sample focused on an age range from 8 to 18 years. A previous study [21] has indicated that, due to the fact that carpal bones start to overlap at around age 7 years in males and 5 years in females, their analysis does not provide accurate and relevant information for subjects older than 7-12 years.

5.2 Future Work

Higher Precision of Specific Indicators

Currently we have 8 indicators that are relatively inaccurate compared with the results from two well trained skeletal-age analysts' visual grading. These indicators are primarily related to the third and fifth metacarpals. The challenge in the analysis of these indicators is that the soft-tissue thickness is always greater in the palm region than in the phalanx region; in addition, the size of the metacarpals is not as large as that of the radius or ulna in the forearm region. All of these issues make the thresholding and edge detection algorithms inaccurate at times. Furthermore, since in the older age range (10-16 years), the margin of the epiphysis near the corresponding metaphysis begins to conform in shape to the end of the metaphysis, and the central part of the end of the metaphysis is convex, the shadow of the epiphysis always overlaps that of the metaphysis. In this particular case, the detection of a relatively radiolucent strip is highly influenced by the overlapped shadows, so the fusion indicators based on this detection become more difficult to be graded. It might be necessary to implement a metacarpal-specific threshold and edge-detection algorithm in order to produce more accurate results.

Assessment of Skeletal Age of Younger Children

As mentioned before, in this study we focused on children in the age group of 8 to 18 years. It would be helpful to implement this automated skeletal-age assessment tool for younger children. In this case, the first problem to be considered will have to be the analysis of the carpal bones. In the FELS method, 31 indicators (31.6% of the total) are related to the carpal bones and were not analyzed in our study. For ages below 5-7 years, the long-bone analysis fails to represent the skeletal development, especially in very young children. This is due to the fact that the epiphysis of the phalanges has not yet been developed nor ossified. However, carpal bone segmentation and feature extraction were proven to be very reliable in this age range,[22] because the carpal bones have not yet started to overlap. Therefore, in order to achieve a reasonable degree of accuracy in skeletal-age assessment for children of younger ages, the features extracted from the carpal region will require attention.

There are 12 additional indicators in the FELS method (12.2% of the total) that were not analyzed in this project. These indicators are unnecessary to be assessed in the age range of this study (8 to 18 years). All of these 12 indicators are concerned with the ossification of the epiphysis, which will be necessary to be graded for ages below 5-7 years. Different grades are assigned if the epiphysis is not ossified or the shape of it is round or flattened. Currently, the highest grades are given to all of these indicators in our automated program by default, considering the age range we worked on. It should be noted that it would be necessary to carefully analyze these indicators in order to improve the accuracy of skeletal age assessment for younger children.

Development of Graphical User Interface

Due to the variability in anatomy, mineralization and image quality across images and within an individual image, a graphical user interface, which can provide the operator with a pictorial view of the algorithm and the program interactions, would be helpful to improve the accuracy of the skeletal age assessment. Such a graphical user interface would provide output of the automated analysis process and include ROI extraction, line profiles and edge detection. In addition, the user interface should offer tools for the operator to correct processes at various stages in case the output of the automatic routines is incorrect.

We can even imagine that, by the end of this series of studies, the computerized skeletal age assessment package for the entire age range, including a graphical user interface, could be integrated into the DXA analysis software. Under these circumstances, the software would allow the user to make a clinical assessment decision right after a DXA left hand/wrist image has been generated.

REFERENCES

1. Tanner J and Whitehouse R (1983): Assessment of skeletal maturity and prediction of adult height, 2nd. ed. Academic Press, London.

2. Greulich WW and Pyle SI (1959): Radiographic atlas of skeletal development of hand and wrist, 2nd. ed. Stanford University Press, California.

3. Concetto Spampinato (1995): Skeletal bone age assessment. University of Catania, Viale Andrea Doria, 6 95125.

4. Roche AF, Chumlea WC and Thissen D (1988): Assessing skeletal maturity of the hand-wrist: FELS method. Springfield: Charles C Thomas. Publisher, pp. 62-77.

5. Chumlea WC, Roche AF and Thissen D (1989): The FELS method of assessing skeletal maturity of the hand-wrist. American Journal of Human Biology, Vol. 1, pp. 175-183.

6. Gertych A, Zhang A, Sayre J (2007): Bone age assessment of children using a digital hand atlas. Computerized Medical Imaging and Graphics 31, pp. 322-331.

7. Greulich WW, Pyle SI (1971): Radiographic atlas of skeletal development of hand wrist. 2ed ed. Stanford, CA: Stanford University Press.

8. Miler G, Levick R and Kay R (1986): Assessment of bone age: A comparison of the Greulich and Pyle and the Tanner and Whitehouse methods. Clin. Radiol. 37, pp. 119-121.

9. Greulich W, Pyle S (1950): Radiographic atlas of skeletal development of the hand and wrist. Stanford Univ. Press, Stanford.

10. Roche AF, Chumlea WC and Thissen D (1988): Assessing skeletal maturity of the hand-wrist: FELS method. Springfield: Charles C Thomas. Publisher, pp. 41-47.

11. Roche AF, Chumlea WC and Thissen D (1988): Assessing skeletal maturity of the hand-wrist: FELS method. Springfield: Charles C Thomas. Publisher, pp. 248-261.

12. Michael DG and Nelson AC (1989): HANDX: A model-based system for automatic segmentation of bones from digital hand radiographs. IEEE Trans. Med. Imag., vol. 8, pp. 64-99.

13. Cheng SNC, Chan H, Niklason LT, and Alder RS (1994): Automated segmentation of regions on hand radiographs. Med. Phys., vol. 21, pp. 1293-1200.

14. Manos GK, Cains AY, Rickets IW, and Sinclair D (1994): Segmenting radiographs of the hand and wrist. Comput. Methods Program Biomed., vol. 43, pp. 227-237.

15. Duryea J, Jiang Y, Countryman P, and Genant HK (1999): Automated algorithm for the identification of join space and phalanx margin location on digital hand radiographs. Med. Phy., vol. 26, pp. 453-461.

16. Raheja AJ (2008): Automated analysis of metacarpal cortical thickness in serial hand radiographs. Wright State University.

17. Otsu N (1979): A threshold selection method from gray-level histograms. IEEE Transaction on Systems, Man and Cybernetics, 1, pp. 62-66.

18. Canny J (1986): A computational approach to edge detection. Pattern Analysis and Machin Intelligence, IEEE Transactions on, PAMI-8(6), pp. 679-698.

19. Onge S, Pierr M and Wang J (2004): Dual-energy x-ray absorptiometry-measured lean soft tissue mass. The Journals of Gerontology: Series A 59 (8), pp. 796-800

20. Gilsanz V(1998). Radiol EJ 26, pp. 177-182

21. Chang CH and Hsieh CW (2003): A fully automatic computerized bone age assessment procedure based on phalange ossification analysis. CVGIP, Kinmen, ROC, pp. 463-468.

22. Johnston FE and Jahina SB (1965): The contribution of the carpal bones to the assessment of skeletal age. Amer, J. Phys. Anthrop., vol. 23, pp. 349-354.

Appendix I

The format of the TXT file, which is used to save grades of indicators of one individual and then run through the PASCAL program in order to estimate skeletal age and standard error:

Ptmo 1-4 r1 14 r3 16 r4 18 r5 20 r6 22 r7 24 r8 26 u1 28 u3 30 c1 32 c2 34 c3 36 c4 38 h1 40 h2 42 h3 44 h4 46 tri1 48 tri2 50 tri3 52 tri4 54 p1 56 l1 58 l2 60 s1 62 s2 64 s3 66 tpm1 68 tpm2 70 tpm3 72 tpm4 74 tpm5 76 tpd1 78 tpd2 80 tpd3 82 tpd4 84 tpd5 86 tpd6 88 tpd7 90 as1 92 me11 94 me13 96 me14 98 me15 100 me16 102 me16 104 me31 106 me33 108 me34 110 me35 112 me51 114 me53 116 me54 118 me55 120 me56 122 pp11 124 pp13 126 pp14 128 pp15 130 pp16 132 pp17 134 pp31 136 pp33 138 pp34 140 pp35 142 pp36 144

Ptno 1-4 pp51 14 pp53 16 pp54 18 pp55 20 mp31 22 mp33 24 mp34 26 mp35 28 mp51 30 mp53 32 mp54 34 mp55 36 dp11 38 dp31 40 dp33 42 dp34 44 dp51 46 dp53 48 dp54 50 +1 r2p3 4.2 +1 u2p3 4.2 +1 me12p3 4.2 +1 me32p3 4.2 +1 me52p3 4.2 +1 pp12p3 4.2 +1 pp32p3 4.2 +1 pp52p3 4.2 +1 mp32p3 4.2 +1 mp52p3 4.2 +1 dp12p3 4.2 +1

Ptno 1-4. +9 dp32p3 4.2 +1 dp52p3 4.2 +1 age 4.1+1 sex 1. +1 assess 2. +1 assessment 1

Appendix II

Indicator	Description	Age Range	Training Set			Testing Set			DXA Set		
			Mean	$2SD_{Mean}$	$\lvert Mean/SD_{Mean} \rvert > 2$	*Mean*	$2SD_{Mean}$	$\lvert Mean/SD_{Mean} \rvert > 2$	*Mean*	$2SD_{Mean}$	$\lvert Mean/SD_{Mean} \rvert > 2$
r2	Ratio of Epiphysis Widths (Radius)	Boys: 0.5 to 12.5 years Girls: 0.5 to 12.5 years	-0.015	0.017	No	-0.036	0.043	No	-0.004	0.032	No
u2	Ratio of Epiphysis Widths (Ulna)	Boys: 7.0 to 13.5 years Girls: 5.5 to 12.0 years	-0.036	0.043	No	-0.015	0.017	No	0.002	0.047	No
me12	Ratio of Epiphysis Widths (Metacarpal I)	Boys: 3.5 to 13.0 years Girls; 1.5 to 13.0 years	-0.019	0.022	No	-0.024	0.023	Yes	-0.025	0.038	No
me32	Ratio of Epiphysis Widths (Metacarpal III)	Boys: 3.0 to 13.5 years Girls: 2.5 to 13.0 years	-0.024	0.025	No	-0.020	0.023	No	0.003	0.022	No
me52	Ratio of Epiphysis Widths (Metacarpal V)	Boys: 1.5 to 16.0 years Girls: 1.0 to 15.0 years	-0.020	0.023	No	-0.019	0.022	No	-0.046	0.050	No
pp12	Ratio of Epiphysis Widths (Proximal phalanx I)	Boys: 2.5 to 13.0 years Girls: 2.5 to 11.0 years	-0.025	0.032	No	0.022	0.020	Yes	-0.027	0.041	No
pp32	Ratio of Epiphysis Widths (Proximal phalanx III)	Boys: 2.5 to 11.5 years Girls: 2.0 to 12.0 years	0.006	0.014	No	-0.025	0.032	No	0.005	0.034	No
pp52	Ratio of Epiphysis Widths (Proximal phalanx V)	Boys: 1.5 to 14.5 years Girls: 0.75 to 14.0 years	0.022	0.020	No	0.006	0.014	No	0.001	0.041	No
mp32	Ratio of Epiphysis Widths (Middle phalanx III)	Boys: 1.5 to 13.5 years Girls: 0.75 to 12.0 years	-0.048	0.016	Yes	-0.037	0.065	No	0.005	0.035	No
mp52	Ratio of Epiphysis Widths (Middle phalanx V)	Boys: 3.5 to 14.0 years Girls: 1.0 to 11.0 years	-0.027	0.030	No	-0.024	0.030	No	-0.027	0.040	No
dp12	Ratio of Epiphysis Widths (Distal phalanx I)	Boys: 1.0 to 12.0 years Girls: 1.5 to 11.0 years	-0.019	0.043	No	-0.027	0.030	No	0.008	0.045	No
dp32	Ratio of Epiphysis Widths (Distal phalanx III)	Boys: 2.5 to 10.5 years Girls: 1.5 to 20.0 years	-0.024	0.030	No	-0.019	0.043	No	-0.024	0.065	No

Indicator	Description	Age Range	Training Set			Testing Set			DXA Set		
			Mean	$2SD_{Mean}$	$\lvert Mean/SD_{Mean}\rvert >2$	*Mean*	$2SD_{Mean}$	$\lvert Mean/SD_{Mean}\rvert >2$	*Mean*	$2SD_{Mean}$	$\lvert Mean/SD_{Mean}\rvert >2$
dp52	Ratio of Epiphysis Widths (Distal phalanx V)	Boys: 2.5 to 11.0 years Girls: 1.5 to 10.5 years	-0.037	0.065	No	-0.043	0.046	No	-0.050	0.049	Yes
r6	Epiphysis/Metaphysis Fusion (Medial third of radius)	Boys: 10.0 to 22.0 years Girls: 8.5 to 22.0 years	0.060	0.063	No	0.015	0.103	No	-0.017	0.100	No
r7	Epiphysis/Metaphysis Fusion (Lateral third of radius)	Boys: 11.0 to 22.0 years Girls: 9.0 to 22.0 years	0.038	0.057	No	0.032	0.095	No	0.035	0.110	No
r8	Epiphysis/Metaphysis Fusion (Central third of radius)	Boys: 13.5 to 20.0 years Girls: 12.0 to 20.0 years	0.034	0.085	No	0.051	0.134	No	0.111	0.152	No
u3	Epiphysis/Metaphysis Fusion (Ulna)	Boys: 15.5 to 22.0 years Girls: 13.5 to 20.0 years	0.073	0.082	No	0.111	0.125	No	0.120	0.160	No
me17	Epiphysis/Metaphysis Fusion (Metacarpal I)	Boys: 13.0 to 20.0 years Girls: 10.0 to 20.0 years	0.046	0.052	No	0.100	0.118	No	0.049	0.088	No
me35	Epiphysis/Metaphysis Fusion (Metacarpal III)	Boys: 13.5 to 22.0 years Girls: 8.5 to 18.0 years	0.087	0.090	No	0.058	0.130	No	0.083	0.106	No
me55	Epiphysis/Metaphysis Fusion (Metacarpal V)	Boys: 10.5 to 20.0 years Girls: 10.0 to 20.0 years	0.162	0.116	Yes	0.138	0.125	Yes	0.151	0.136	Yes
pp15	Epiphysis/Metaphysis Fusion (Proximal phalanx I)	Boys: 13.5 to 20.0 years Girls: 10.5 to 16.5 years	0.019	0.037	No	0.050	0.152	No	0.027	0.152	No
pp35	Epiphysis/Metaphysis Fusion (Proximal phalanx III)	Boys: 13.5 to 22.0 years Girls: 10.5 to 16.5 years	0.074	0.104	No	0.075	0.157	No	-0.081	0.124	No
pp55	Epiphysis/Metaphysis Fusion (Proximal phalanx V)	Boys: 13.0 to 20.0 years Girls: 10.5 to 17.5 years	0.131	0.138	No	0.083	0.094	No	0.051	0.107	No

Indicator	Description	Age Range	Training Set			Testing Set			DXA Set		
			Mean	$2SD_{Mean}$	$\|Mean/SD_{Mean}\| >2$	*Mean*	$2SD_{Mean}$	$\|Mean/SD_{Mean}\| >2$	*Mean*	SD_{Mean}	$\|Mean/SD_{Mean}\| >2$
mp35	Epiphysis/Metaphysis Fusion (Middle phalanx III)	Boys: 13.0 to 20.0years Girls: 10.5 to 16.5 years	0.069	0.083	No	0.133	0.113	Yes	0.146	0.139	Yes
mp55	Epiphysis/Metaphysis Fusion (Middle phalanx V)	Boys: 13.0 to 22.0 years Girls: 10.5 to 20.0 years	0.063	0.089	No	0.122	0.123	No	0.133	0.163	No
dp14	Epiphysis/Metaphysis Fusion (Distal phalanx I)	Boys: 12.0 to 18.0 years Girls: 10.5 to 15.5 years	0.054	0.079	No	0.128	0.144	No	0.119	0.155	No
dp34	Epiphysis/Metaphysis Fusion (Distal phalanx III)	Boys: 13.0 to 20.0 years Girls: 10.5 to 17.0 years	0.066	0.092	No	0.063	0.110	No	0.068	0.120	No
dp54	Epiphysis/Metaphysis Fusion (Distal phalanx V)	Boys: 13.0 to 22.0 years Girls: 10.0 to 16.5 years	0.068	0.095	No	0.043	0.107	No	0.048	0.107	No
r4	Radiopaque Line on Epiphysis (Distal margin. Radius)	Boys: 0.5 to 8.0 years Girls: 0.75 to 6.0 years	0.000	0.000	No	0.000	0.000	No	0.000	0.000	No
me33	Radiopaque Line on Epiphysis (Lateral margin. Metacarpal III)	Boys: 5.5 to 22.0 years Girls: 6.0 to 15.0 years	-0.063	0.054	Yes	-0.089	0.083	Yes	-0.083	0.098	No
me53	Radiopaque Line on Epiphysis (Lateral margin. Metacarpal V)	Boys: 7.5 to 15.5 years Girls: 5.0 to 13.0 years	0.040	0.127	No	0.041	0.142	No	0.047	0.128	No
pp14	Radiopaque Line on Epiphysis (Proximal margin. Proximal Phalanx I)	Boys: 6.5 to 16.5 years Girls: 4.0 to 14.0 years	-0.094	0.081	Yes	-0.102	0.094	Yes	-0.093	0.092	Yes

Indicator	Description	Age Range	Training Set			Testing Set			DXA Set		
			Mean	$2SD_{Mean}$	$\lvert Mean/SD_{Mean}\rvert >2$	*Mean*	$2SD_{Mean}$	$\lvert Mean/SD_{Mean}\rvert >2$	*Mean*	$2SD_{Mean}$	$\lvert Mean/SD_{Mean}\rvert >2$
pp34	Radiopaque Line on Epiphysis (Proximal margin. Proximal Phalanx III)	Boys: 6.0 to 14.0 years Girls: 4.0 to 14.5 years	-0.042	0.083	No	-0.114	0.122	No	-0.105	0.131	No
pp54	Radiopaque Line on Epiphysis (Proximal margin. Proximal Phalanx V)	Boys: 8.0 to 16.5 years Girls: 7.0 to 14.5 years	0.019	0.126	No	-0.100	0.133	No	-0.041	0.104	No
mp33	Radiopaque Line on Epiphysis (Middle Phalanx III)	Boys: 1.5 to 10.5 years Girls: 1.5 to 10.5 years	0.000	0.000	No	0.000	0.000	No	0.000	0.000	No
mp53	Radiopaque Line on Epiphysis (Middle Phalanx V)	Boys: 2.5 to 10.0 years Girls: 1.5 to 8.5 years	0.091	0.182	No	-0.091	0.223	No	-0.040	0.235	No
dp33	Radiopaque Line on Epiphysis (Distal Phalanx III)	Boys: 2.5 to 13.0 years Girls: 2.0 to 11.5 years	0.056	0.077	No	-0.056	0.127	No	-0.100	0.150	No
dp53	Radiopaque Line on Epiphysis (Distal Phalanx III)	Boys: 2.5 to 13.0 years Girls: 2.0 to 11.5 years	0.077	0.086	No	-0.050	0.125	No	-0.088	0.156	No
r5	Shape of Radiopaque Line (Radius)	Boys: 10.0 to 22.0 years Girls: 8.5 to 22.0 years	0.040	0.182	No	0.043	0.158	No	0.050	0.178	No
me14	Proximal Margin of Epiphysis (Metacarpal I)	Boys: 3.5 to 13.5 years Girls: 3.0 to 12.0 years	0.094	0.138	No	0.029	0.103	No	0.000	0.099	No
me16	Distal Margin of Epiphysis (Metacarpal I)	Boys: 3.5 to 13.5 years Girls: 3.0 to 12.0 years	0.079	0.079	Yes	0.031	0.082	No	0.054	0.116	No
me56	Medial Margin of Epiphysis (Metacarpal V)	Boys: 8.5 to 22.0 years Girls: 8.0 to 22.0 years	-0.073	0.072	Yes	-0.070	0.155	No	-0.108	0.140	No

Indicator	Description	Age Range	Training Set			Testing Set			DXA Set		
			Mean	$2SD_{Mean}$	$\lvert Mean/SD_{Mean}\rvert >2$	*Mean*	$2SD_{Mean}$	$\lvert Mean/SD_{Mean}\rvert >2$	*Mean*	$2SD_{Mean}$	$\lvert Mean/SD_{Mean}\rvert >2$
pp13	Proximal Margin of Epiphysis (Proximal phalanx I)	Boys: 1.5 to 10.0 years Girls: 1.0 to 10.0 years	-0.222	0.202	Yes	-0.253	0.231	Yes	-0.257	0.250	Yes
pp16	Distal Margin of Epiphysis (Proximal phalanx I)	Boys: 2.5 to 14.5 years Girls: 0.75 to 11.5 years	0.023	0.103	No	-0.022	0.146	No	-0.026	0.144	No
pp17	Disto-medial Projection (Proximal phalanx I)	Boys: 2.5 to 14.5 years Girls: 0.75 to 11.5 years	0.136	0.105	Yes	0.093	0.086	Yes	0.128	0.120	Yes
pp33	Proximal Margin of Epiphysis (Proximal phalanx III)	Boys: 0.5 to 8.0 years Girls: 0.5 to 7.0 years	0.000	0.000	No	0.000	0.000	No	0.000	0.000	No
pp36	Distal End Shape (Proximal phalanx III)	Boys: 2.5 to 14.5 years Girls: 0.75 to 11.5 years	0.000	0.075	No	-0.024	0.085	No	-0.029	0.100	No
pp53	Proximal Margin of Epiphysis (Proximal phalanx V)	Boys: 0.75 to 9.0 years Girls: 1.0 to 7.0 years	0.000	0.000	No	0.000	0.000	No	0.000	0.000	No
mp34	Distal End Shape (Middle phalanx III)	Boys: 7.5 to 22.0 years Girls: 5.0 to 15.5 years	0.025	0.112	No	-0.029	0.118	No	-0.017	0.130	No
mp54	Distal End Shape (Middle phalanx V)	Boys: 8.5 to 22.0 years Girls: 8.0 to 22.0 years	0.011	0.088	No	-0.070	0.109	No	-0.046	0.111	No